IOPscience

Hydrodynamics of local excitations after an interaction quench in 1D cold atomic gases

You may also be interested in:

Universal dynamics of a soliton after an interaction quench
Fabio Franchini, Andrey Gromov, Manas Kulkarni et al.

Dark-soliton-like excitations in the Yang–Gaudin gas of attractively interacting fermions
Sophie S Shamailov and Joachim Brand

Quantum states of dark solitons in the 1D Bose gas
Jun Sato, Rina Kanamoto, Eriko Kaminishi et al.

Soliton splitting in quenched classical integrable systems
O Gamayun and M Semenyakin

The Universe on a table top: engineering quantum decay of a relativistic scalar field from a metastable vacuum
O Fialko, B Opanchuk, A I Sidorov et al.

Beyond mean-field dynamics of ultra-cold bosonic atoms in higher dimensions: facing the challenges with a multi-configurational approach
V J Bolsinger, S Krönke and P Schmelcher

Engineering bright matter-wave solitons of dipolar condensates
M J Edmonds, T Bland, R Doran et al.

Implementing quantum electrodynamics with ultracold atomic systems
V Kasper, F Hebenstreit, F Jendrzejewski et al.

The quench map in an integrable classical field theory: nonlinear Schrödinger equation
Vincent Caudrelier and Benjamin Doyon

New Journal of Physics

The open access journal at the forefront of physics

CrossMark

PAPER

Hydrodynamics of local excitations after an interaction quench in 1*D* cold atomic gases

Fabio Franchini[1,2,3,8], Manas Kulkarni[4,5] and Andrea Trombettoni[6,7]

1. Ruđer Bošković Institute, Bijenčka cesta 54, 10000 Zagreb, Croatia
2. INFN, Sezione di Firenze, Via G. Sansone 1, I-50019 Sesto Fiorentino (FI), Italy
3. The Adbus Salam ICTP, Strada Costiera 11, I-34151, Trieste, Italy
4. Department of Physics, New York City College of Technology, The City University of New York, Brooklyn, NY 11201, USA
5. International Centre for Theoretical Sciences, Tata Institute of Fundamental Research, Bangalore - 560089, India
6. CNR-IOM DEMOCRITOS Simulation Center, Via Bonomea 265, I-34136 Trieste, Italy
7. SISSA and INFN, Sezione di Trieste, Via Bonomea 265, I-34136 Trieste, Italy
8. Author to whom any correspondence should be addressed.

E-mail: gfabio@gmail.com, manas.kulkarni@icts.res.in and andreatr@sissa.it

Abstract

We discuss the hydrodynamic approach to the study of the time evolution—induced by a quench—of local excitations in one dimension. We focus on interaction quenches: the considered protocol consists of creating a stable localized excitation propagating through the system, and then operating a sudden change of the interaction between the particles. To highlight the effect of the quench, we take the initial excitation to be a soliton. The quench splits the excitation into two packets moving in opposite directions, whose characteristics for short times can be expressed in a universal way. Our treatment allows for the description of the internal dynamics of these two packets in terms of the different velocities of their components. We confirm our analytical predictions through numerical simulations performed with the Gross–Pitaevskii equation and with the Calogero model (as an example of long range interactions and solvable with a parabolic confinement). Through the Calogero model we also discuss the effect of an external trapping on the protocol. The hydrodynamic approach shows that there is a difference between the bulk velocities of the propagating packets and the velocities of their peaks: it is possible to discriminate the two quantities, as we show through the comparison between numerical simulations and analytical estimates. We show that our analytical results capture with remarkable precision the findings of the numerical simulations also for intermediate times and we provide predictions for the time at which the two packets becomes distinguishable. In the realizations of the discussed quench protocol in a cold atom experiment, these different velocities are accessible through different measurement procedures.

1. Introduction

The outstanding performances of modern experiments in preparing and controlling setups of quantum gases [1, 2] have promoted the study of out-of-equilibrium systems in ultracold gases as arguably one of the most challenging topics in the field [3–18]. One of the reasons for the complexity of this challenge is due to the variety of ways in which a system can be driven out of equilibrium and the difficulty in having a general guidance principle to relate their phenomenologies.

Thus, over the years, the community has concentrated on a few protocols that have emerged to be sufficiently clean and interesting. One question at the forefront has been under which conditions (and in which sense) a system is able to reach an equilibrium, and whether this equilibrium can show universal characteristics such as thermalization [19–29]. Particularly useful in addressing such questions are setups based on cold atoms [30–36].

One of the most experimentally relevant protocols to study out-of-equilibrium dynamics and the issue of thermalization is the quench protocol in which, typically, a system described by a Hamiltonian H is prepared in its ground state and then, at a given moment of time, is evolved using a different Hamiltonian H' [37]. The questions usually asked with quantum quenches refer to late times properties of the systems (and whether the unitary evolution can lead to something that can locally be described in a semi-classical way) [38–42].

Variations to the usual quench protocol have been considered typically in two forms: the initial state was taken to be an excited state of the initial Hamiltonian [43], or the interaction was changed only locally [44–48]. In a recent work [35], we introduced a different protocol: we proposed to start with a local excitation and to let it evolve after a global interaction quench. In order to isolate the effect of the quench on the dynamics, the initial state is prepared as a solitonic excitation of the original Hamiltonian, that is, a state for which the one-particle density profile evolves without (almost) changing its shape. This setup has the merit of being experimentally feasible and of showing universal properties already at short times. In [35] it was also shown that, by changing the underlying interaction during soliton motion, the excitation breaks into two profiles: one moving in the same direction as the initial excitation, the other in the opposite. In a cold atom setup, such a quench can be triggered through trapping or with an external magnetic field [1] to induce a change in the scattering length and in the speed of sound. The system is then allowed to evolve for short times after the quench and the velocities and shapes of the two chiral profiles created by the quench can be measured either by direct imaging or reconstructed by releasing the trap, through time-of-flight measurements.

As we are going to discuss in this paper, a convenient way to study the dynamics of a local excitation is to employ a (non-linear) hydrodynamics description of the system in terms of the density and velocity fields. Moreover, if the initial density profile is not a large perturbation over the background, velocities and shapes of the transmitted and reflected profiles for short times after the quench can be expressed in a universal way, that is independent from the details of the quench and of the microscopic interaction [35]. The hydrodynamic approach [49] is complementary to a microscopic computation of the dynamics (when practically doable), and it has the advantage that microscopic details of the underlying model enter as parameters of the hydrodynamic equation (e.g., the sound velocity). It also provides a standard tool to study collective excitations and dynamical properties in cold atom setups [50, 51] and it applies as well to higher dimensions: however in this paper, in line with the topic of this Focus Issue and with our choice to consider solitonic solutions we limit ourself to one dimensional systems and soliton excitations (in higher dimensions, solitonic states are stable only for limited times and one needs to take into account the spreading and the excitations of the wave packet). We consider in detail the Gross–Pitaevskii (GP) equation, with δ-like interactions (which is relevant for the $1D$ Bose gases in the limit of small interactions [50]), and the Calogero model, since it is exactly solvable also with in the presence of a parabolic trapping potential [52–54].

The same quench setup has also been considered in [55–57] with a specific interest on integrable PDEs describing the evolution of one dimensional systems and on the translation of the quench protocol in the corresponding quantum inverse scattering problem. These papers signal the interest of the community in the interaction quench. We would like to stress that the proposed quench protocol could be implemented relatively easily in cold atoms experiments and that, by focusing on the short time universal dynamics, our predictions can be tested directly in the laboratory, which should be contrasted with typical large time results produced by other approaches and protocols. Universal properties of short time out-of-equilibrium dynamics has been considered in [35, 58–60].

In this work our main goal is to investigate in detail the hydrodynamic approach for the study of the dynamics of solitonic excitations in one-dimensional systems, clarifying the hypothesis behind the derivations based on the hydrodynamic approach and to discuss the possible experimental realization of the quench protocol in cold atom systems. To the latter aim, we address an important issue related to the measurability of the chiral profiles generated by the quench and relevant for the cold atom physical realizations. In fact, at the quench time the transmitted and reflected profiles are perfectly overlapping and can be distinguished only after they have moved apart. While in time-of-flight experiments one need not wait this time, since the two profiles have opposite momentum, in a real imaging scenario (such as that we employ in our numerical experiments) this waiting time can introduce additional effects. We analytically estimate this waiting time. Moreover, since the two chiral profiles are not solitons of the post-quench system, the center-of-mass (average) velocity of each profile might be different from the velocity of its highest point. We find that in the hydrodynamic approach one can naturally introduce both 'bulk' and 'peak' velocities of the transmitted and reflected packets: we provide expressions for both quantities, and we compare them with our numerical simulations for the GP and Calogero models. We also discuss the time scales relevant for the experimental realization of the proposed protocol and the efficacy of our approximation within them.

The plan of the paper is as follows. In section 2 we review the hydrodynamic approach to the description of one dimensional cold atomic gases [51]. In section 3 we analyze the quench protocol and derive the expressions for the velocities and heights of the chiral profiles generated by the quench. In sections 3.1 and 3.2 we compare

the analytical prediction against our numerical simulations performed on the one-dimensional GP equation and on the Calogero model. In section 4 we discuss our results and comment on future perspectives. Finally, we collect some useful (although more technical) information in the appendices. Appendix A explains how we can extract an integrable dynamics out of a generic hydrodynamic system, while in appendix B we discuss the main properties of the integrable core, the Korteweg–de Vries (KdV) equation. In appendices C we discuss some different versions of the 1*D* GP and their relation to KdV. Finally, in appendices D and E we collect the basic facts about the rational Calogero model and its version confined in a harmonic potential (also integrable).

2. The hydrodynamic approach

All quantum systems at sufficiently low temperature acquire a collective behavior. In many such cases, the expectation value of the particle density operator $\hat{\rho}(x) = \sum_j \delta(x - x_j)$ becomes a smooth function and the quantum fluctuations around it are negligible. When this happens, the system dynamics can be described with a hydrodynamic approach [49]. In the following, we will primarily be interested in one dimensional systems with one particle species without additional internal degrees of freedom, so that it is sufficient to introduce the scalar density $\rho(x, t)$ and velocity $v(x, t)$ fields.

Assuming Galilean invariance and locality, the most general hydrodynamic Hamiltonian reads [51]

$$H = \int dx \left[\frac{\rho v^2}{2} + \rho \epsilon(\rho) + A(\rho) \frac{(\partial_x \rho)^2}{4\rho} \right], \tag{1}$$

where $\epsilon(\rho)$ is the internal energy and $A(\rho)$ is related to quantum pressure. We also assume that dissipative effects can be neglected. The equations of motions can be obtained by remembering that the density and velocity are conjugated fields [61, 62] satisfying

$$\{\rho(x), v(y)\} = \partial_x \delta(x - y). \tag{2}$$

They are the continuity and Euler equations [49]:

$$\dot{\rho} + \partial(\rho v) = 0; \quad \dot{v} + \partial \mathcal{A} = 0 \tag{3}$$

$$\mathcal{A} \equiv \frac{v^2}{2} + \omega(\rho) - A'(\rho)(\partial \sqrt{\rho})^2 - A(\rho) \frac{\partial^2 \sqrt{\rho}}{\sqrt{\rho}}, \tag{4}$$

where $\omega(\rho) = \partial_\rho(\rho \epsilon(\rho))$ is the specific enthalpy (which at zero temperature reduces to the chemical potential).

Under the foretold conditions, these equations are completely general: the functions $\epsilon(\rho)$ and $A(\rho)$ encode the specificity of the system under consideration. A discussion of how one can extract an integrable dynamics out of a generic hydrodynamic system and the derivation of the KdV (used in the next section) is reported in appendix A, and useful facts about the KdV are in appendix B.

Choosing

$$\epsilon = \frac{g}{2m} \rho, \qquad A = \frac{\hbar^2}{2m}, \tag{5}$$

and combining the hydrodynamic fields into the complex field

$$\Psi = \sqrt{\rho} \, e^{i\frac{m}{\hbar} \int^x v(y) dy} \tag{6}$$

the dynamical equations (3), (4) can be written as the single complex equation

$$i\hbar \partial_t \Psi(x, t) = \left\{ -\frac{\hbar^2}{2m} \partial_{xx} + g(|\psi(x, t)|^2 - \rho_0) \right\} \psi(x, t), \tag{7}$$

which can be recognized as the 1*D* non-linear Schrödinger equation, aka the 1*D* GP equation (without the external potential in (7)). In equation (7) ρ_0 is the density for $x \to \infty$. Details about the the non-linear Schrödinger equation and its KdV reduction are in appendix C.

The GP equation has been routinely used in the last two decades to describe the dynamics of ultracold bosons at $T = 0$ [50]. In 3*D* its validity stems from the fact that there is a condensate, whose macroscopic wavefunction obeys the GP equation, from which one can derive hydrodynamic equations [50]. In 1*D* there is no condensate, since there is actually a 'quasi-condensate' [63]: however, the GP gives a good description of experimental results for small interactions (i.e., for the coupling constant of the Lieb–Liniger model, defined in (C1), $\gamma = \frac{m}{\hbar^2} \frac{g}{\rho_0} \ll 1$ [64]) and in particular of the—dark and bright—soliton dynamics observed in 1*D* experiments [65, 66] and of shock waves [67]. When in 1*D* the coupling constant is not much smaller than 1, one can nevertheless use hydrodynamic classical equations (as the ones given above) to study small deviations from equilibrium [68]. For larger deviations one has to study the quantum dynamics directly using the Lieb–Liniger model (which might be

at present rather challenging from the computational point of view) or resort to $1D$ mean-field effective equations [69–72] from which hydrodynamic equations may be derived as above producing (time-dependent) non-linear Schrödinger equations with suitable general non-linear terms $\epsilon(\rho)$, the GP equation corresponding to $\epsilon(\rho) \propto \rho$. As discussed in [35] a good agreement is found between the hydrodynamic results and the GP equation with a power-law $\epsilon(\rho)$. We observe that such mean-field equations may fail in correctly describing interference between wavepackets, as shown for the Tonks–Girardeau limit $\gamma \to \infty$ in [73]: in general one expects anyway that the mean-field equations work better at short times with respect to long times. For instance, the long-time fate of a soliton configuration due to classical to quantum crossover has been studied in [74].

3. The quench protocol

In this section we discuss in detail the quench protocol. The starting point is to prepare the system with a localized excitation. In general, since such a state cannot be an eigenstate of a translational invariant system, in time it would diffuse and disperse. However, it is an empirical observation that several systems abruptly taken away from equilibrium, settle back in configurations displaying localized excitations that propagates for long times without degrading significantly. Such behavior is that of a soliton (or trains of solitons) and it is a manifestation of the emergent collective hydrodynamics ensuing in the system. True solitons are a characteristic feature only of integrable differential equations [75]. Nonetheless, individual (or well separated) solitonic waves are commonly observed in a variety of systems, including of course classical systems [76] and ultracold systems [77].

For the quantum many-body Lieb–Liniger model of interacting bosons in $1D$ it is not obvious what is the quantum content of the microscopical state that results into a soliton. It makes sense that it would contain a large number of eigenstates such that the coherent dynamics prevents their macroscopic spreading, similarly to what happens in quadratic theories for coherent states. Indeed, the construction of quantum states with one particle density evolving in a solitonic way has not provided conclusive results so far [78–80], in the sense that it is not clear what is the definition of a quantum dark soliton from the Bethe ansatz solution, and if the quantum dark soliton may be defined at all (see however the very recent discussion in [81]).

In this work we do not try to solve this problem, but we hope that our analysis can contribute in this direction. Our starting point is the empirical observation that solitonic configurations are commonly excited (and manipulated) in cold atomic Bose [65, 66, 77, 82] and Fermi [83] systems and that they are best understood in terms of an effective semi-classical hydrodynamical description of the system.
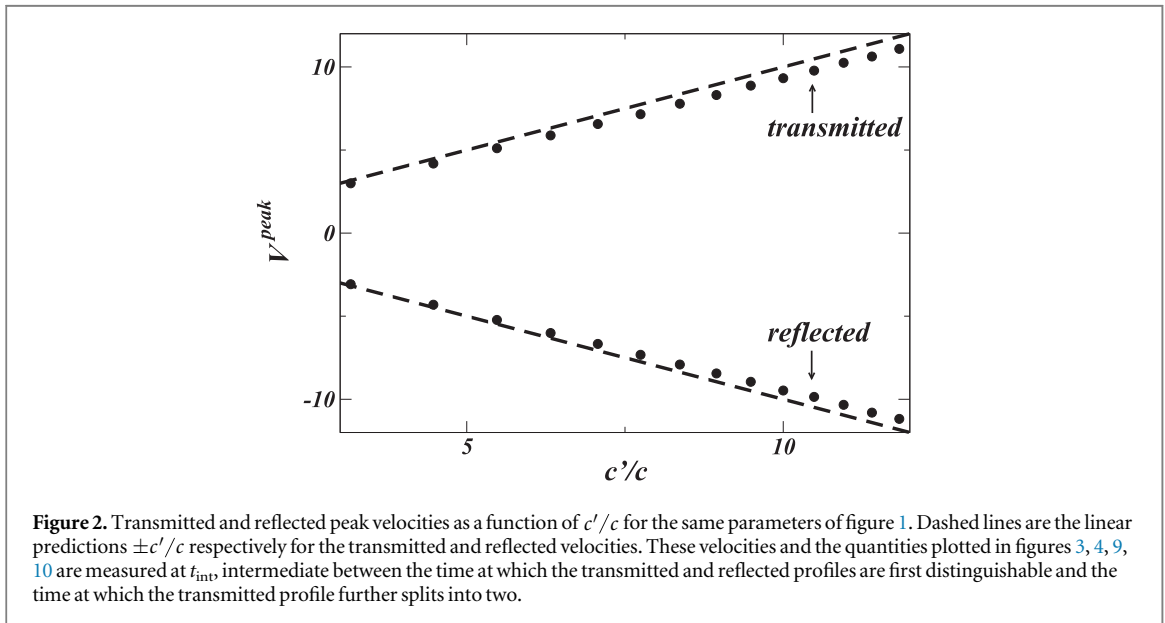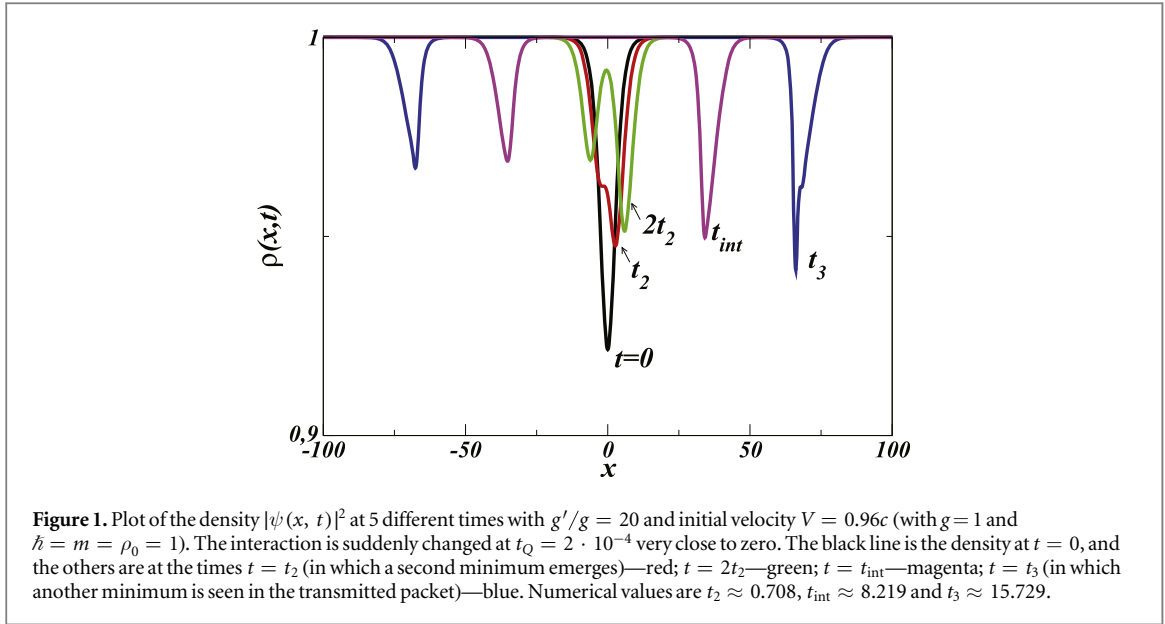
Once a solitonic excitation is created, its density profile will remain (approximately) constant and will only translate in space at a constant velocity. In our quench protocol, at some time during the soliton evolution we change the parameter g governing the interaction strength of the system to g'. This interaction quench modifies the hydrodynamic equations so that the initial soliton cannot evolve unperturbed anymore. We aim at describing the dynamics, and in particular the short time dynamics, of the soliton after the quench.

To qualitatively illustrate what happens after an interaction quench, we take as an example the GP equation (7) and we change the interaction parameter g to a value $g' > g$ at the time t_Q. The sound velocity changes from $c = \sqrt{g}$ to $c' = \sqrt{g'}$ (in units where $\hbar = m = \rho_0 = 1$ where ρ_0 is the density for $x \to \infty$). As the initial condition we take the gray soliton with velocity V [50, 84] reported in appendix C

$$\psi(x, t = 0) = i\,\frac{V}{c} + \gamma \tanh \gamma c x, \tag{8}$$

where $\gamma = \sqrt{1 - V^2/c^2}$. As illustrated in figure 1 there is a time t_2 at which the soliton splits in two (more precisely: at which a second minimum is seen), and a time t_3 in which another splits occurs and one of the two packets in turn splits in two as well. We also define an intermediate time $t_{\text{int}} = (t_2 + t_3)/2$. The numerical values of the transmitted and reflected velocities are plotted in figure 2: these numerical values are obtained by computing the velocities of the (transmitted and reflected) peaks from the peak positions around t_{int}, which reduces numerical fluctuations (as we discuss later and show in figure 5, we verified that between t_2 and t_3 the peak velocities are rather stable, while close to t_2 and t_3 numerical fluctuations may be present).

In figure 2 we plot the analytical prediction $\pm c'/c$ obtained from a linear approximation (as discussed below), where the $+(-)$ is for the transmitted (reflected) components. The hydrodynamic approach we introduce in the following reproduces the leading behavior and it is found to be able to reproduce deviations from it. It is also possible to use the hydrodynamic approach to discriminate the bulk and peak velocities: indeed, from the hydrodynamic theory one has that for very short times after the interaction (well before t_2 where a second minimum is observable) the transmitted and reflected packet move as transmitted and reflected solitons. The numerical findings we present in the following confirm the validity of the hydrodynamic results up to the time scale t_{int}.

Figure 1. Plot of the density $|\psi(x, t)|^2$ at 5 different times with $g'/g = 20$ and initial velocity $V = 0.96c$ (with $g = 1$ and $\hbar = m = \rho_0 = 1$). The interaction is suddenly changed at $t_Q = 2 \cdot 10^{-4}$ very close to zero. The black line is the density at $t = 0$, and the others are at the times $t = t_2$ (in which a second minimum emerges)—red; $t = 2t_2$—green; $t = t_{\mathrm{int}}$—magenta; $t = t_3$ (in which another minimum is seen in the transmitted packet)—blue. Numerical values are $t_2 \approx 0.708$, $t_{\mathrm{int}} \approx 8.219$ and $t_3 \approx 15.729$.

Figure 2. Transmitted and reflected peak velocities as a function of c'/c for the same parameters of figure 1. Dashed lines are the linear predictions $\pm c'/c$ respectively for the transmitted and reflected velocities. These velocities and the quantities plotted in figures 3, 4, 9, 10 are measured at t_{int}, intermediate between the time at which the transmitted and reflected profiles are first distinguishable and the time at which the transmitted profile further splits into two.

To set up the hydrodynamic approach for the propagation of the localized excitations after the interaction quench, as we argued above we take the dynamics before the quench to be captured by the equations (3), (4), where the hydrodynamic parameters $\omega(\rho; g)$ and $A(\rho; g)$ depend on a microscopical parameter g, setting the strength of the inter-particle interaction. The shape of the initial soliton is set by the coupling g and by its velocity V. The approach we develop in this section is independent from the microscopic details and it applies to general $1D$ systems with solitonic excitations, and it will be compared with numerical results in the next sections.

The existence of a soliton is a strong indication that it is possible to isolate out of (3), (4) an integrable core, with the remaining terms being negligible for a relatively long time. If the initial soliton has velocity V close to the speed of sound c (so that its amplitude is also small compared to the background density ρ_0), it is known that the hydrodynamics can be reduced to that of the integrable KdV. We outline the reduction of equations (3), (4) to KdV in appendix A. This procedure, developed for cold atoms in [51], is at the heart of our analysis and thus in the following we assume $\frac{V}{c} \simeq 1$.

The KdV is a chiral equation that reads

$$\dot{u}_\pm \mp \partial_x \left[c u_\pm + \frac{\zeta}{2} u_\pm^2 - \alpha \partial_x^2 u_\pm \right] = 0, \tag{9}$$

where $c \equiv \sqrt{\rho_0 \omega_0'}$ is the sound velocity ($\omega_0' \equiv \partial_\rho \omega|_{\rho_0}$) and the nonlinear and dispersive coefficients are given by

$$\zeta \equiv \frac{c}{\rho_0} + \frac{\partial c}{\partial \rho_0}, \qquad \alpha \equiv \frac{A(\rho_0)}{4c}. \tag{10}$$

Details on the derivation of the KdV equation in a generic hydrodynamic system are given in appendix A.

The $\pm$ in (9) refers to the two chiralities of the waves while $u(x, t)$ is approximately the density fluctuation over the background $u \simeq \rho - \rho_0$. The KdV reduction neglects the interaction between the left and right moving sectors. Due to locality, such approximation is violated only when the two chiral profiles overlap. However, since they move with relative velocity of approximately $2c$, such effects exists only for short times and hence can be neglected [84].

Suddenly during the evolution of the soliton, we change the interparticle coupling to g'. Thus, after the quench the hydrodynamic equations will change and the effective dynamics will be given by the KdV (9) with modified parameters ζ', α' and a new speed of sound c'. This sudden change in the interaction is seen by the soliton profile as a perturbation to which it reacts by splitting into a transmitted and reflected profile, exactly as it would happen to a linear wave, in the presence of an obstacle, or if the sound velocity is suddenly changed.

Before the quench, the initial state can be approximated by the KdV soliton (B5)

$$u(x, t) = s(x - Vt). \tag{11}$$

We make the ansatz that after the quench

$$u(x, t) = u_r(x - V_r t) + u_t(x - V_t t), \tag{12}$$

that is, we assume that the quench acts as an external force which splits the soliton into a transmitted and a reflected profile and that, for short times after the quench, these bumps evolve with a given velocity, without changing their shape significantly. If $V > 0$, the reflected velocity $V_r < 0$ and the transmitted one is $V_t > 0$. Imposing continuity of the solution and conservation of momentum at $t = 0$ we obtain

$$u(x, t) = R(V, V_r, V_t) s(x - V_r t) + T(V, V_r, V_t) s(x - V_t t), \tag{13}$$

with

$$R(V, V_r, V_t) = \frac{V_t - V}{V_t - V_r}, \qquad \text{and} \qquad T(V, V_r, V_t) = \frac{V - V_r}{V_t - V_r}. \tag{14}$$

Note that, applying the same quench protocol to an initial sound wave moving at the pre-quench speed of sound c would yield transmitted and reflected waves moving at the post-quench sound speed $\pm c'$. The above formulae specialize for this case to

$$R_{\text{linear}} = \frac{c' - c}{2 c'} = \frac{1}{2}\left[1 - \frac{c}{c'}\right], \qquad \text{and} \qquad T_{\text{linear}} = \frac{c' + c}{2 c'} = \frac{1}{2}\left[1 + \frac{c}{c'}\right]. \tag{15}$$

The derivation of (13), (14) is completely general, based only on the ansatz that after the quench the soliton splits into two chiral profiles, and does not depend on the dynamics. The laws governing the evolutions are needed to determine the velocities of the two profiles.

We can estimate the profiles velocities by looking at the motion of their center-of-mass[9]

$$\langle x \rangle_u = \frac{\int x \, u \, \mathrm{d}x}{\int u \, \mathrm{d}x}. \tag{16}$$

The velocities are thus

$$V_{r,t} = \partial_t \langle x \rangle_{u_{r,t}} = \frac{1}{\int u_{r,t} \, \mathrm{d}x} \int x \, \dot{u}_{r,t} \, \mathrm{d}x, \tag{17}$$

where we used the fact that the denominator is the integral of motion I_0 (B8) and thus does not evolve with time. We can trade the time derivative for a spacial one through the post-quench equation of motion (9):

$$V_{r,t} = \pm \frac{1}{\int u_{r,t} \, \mathrm{d}x} \int x \, \partial_x \left[c' u_{r,t} + \frac{\zeta'}{2} u_{r,t}^2 - \alpha' \partial_x^2 u_{r,t} \right] \mathrm{d}x, \tag{18}$$

where the $+ (-)$ sign applies to the left (right) moving profile. We can now integrate by part (remembering that at large distances the profiles decay to zero exponentially) to get

---

[9] We thank the referee for suggesting this approach.

$$V_{r,t} = \mp \frac{\int \left[c' u_{r,t} + \frac{\zeta'}{2} u_{r,t}^2 \right] \mathrm{d}x}{\int u_{r,t} \, \mathrm{d}x} = \mp \left[c' + \frac{\zeta'}{2} \frac{\int u_{r,t}^2 \mathrm{d}x}{\int u_{r,t} \, \mathrm{d}x} \right]. \tag{19}$$

Note that this expression has a natural interpretation as the ratio between the first two integrals of motion (B8), (B9), which can be interpreted as the mass and momentum. Indeed, in (B11) we show that this is the case for a soliton:

$$c - V = \frac{I_1}{I_0} = \frac{\zeta}{2} \frac{\int s^2 \mathrm{d}x}{\int |s| \mathrm{d}x}. \tag{20}$$

The integral of motions of the two profiles after the quench are determined immediately at their creation and, remembering (13), are simple rescaling of the original ones:

$$V_r = -c' + \frac{\zeta'}{2} \frac{\int u_r^2 \mathrm{d}x}{\int |u_r| \mathrm{d}x} = -c' + R \frac{\zeta'}{2} \frac{\int s^2 \mathrm{d}x}{\int |s| \mathrm{d}x}, \tag{21}$$

$$V_t = c' - \frac{\zeta'}{2} \frac{\int u_t^2 \mathrm{d}x}{\int |u_t| \mathrm{d}x} = c' - T \frac{\zeta'}{2} \frac{\int s^2 \mathrm{d}x}{\int |s| \mathrm{d}x}. \tag{22}$$

We can now use (20) and (14) to get

$$V_r = -c' + \frac{\zeta'}{\zeta} \frac{V_t - V}{V_t - V_r} (c - V), \tag{23}$$

$$V_t = c' - \frac{\zeta'}{\zeta} \frac{V - V_r}{V_t - V_r} (c - V). \tag{24}$$

Solving this system we finally get

$$V_r = -[c - \eta \, R \, (c - V)] \frac{c'}{c}, \tag{25}$$

$$V_t = [c - \eta \, T \, (c - V)] \frac{c'}{c}, \tag{26}$$

where we introduced the universal parameter

$$\eta \equiv \frac{c}{c'} \frac{\zeta'}{\zeta} = \frac{1 + \frac{\rho_0}{c'} \frac{\partial c'}{\partial \rho_0}}{1 + \frac{\rho_0}{c} \frac{\partial c}{\partial \rho_0}}, \tag{27}$$

and where the *T* and *R* are found consistently to be

$$R = \frac{1}{2} \left[1 - \frac{c}{c'} \frac{V}{\eta \, V + (1 - \eta) \, c} \right], \tag{28}$$

$$T = \frac{1}{2} \left[1 + \frac{c}{c'} \frac{V}{\eta \, V + (1 - \eta) \, c} \right]. \tag{29}$$

We note that these expressions are completely universal. Equations (25)–(29) already appeared in [35] with a different, more qualitative, derivation.

   To further highlight the universality of equations (25)–(29), we can make everything dimensionless, by measuring velocities in units of sound velocity. Thus, we introduce the *reduced velocities*:

$$\nu \equiv \frac{c - V}{c}, \qquad \nu_r \equiv \frac{c' + V_r}{c'}, \qquad \text{and} \qquad \nu_t \equiv \frac{c' - V_t}{c'}, \tag{30}$$

and we write (25), (26) as

$$\nu_r = \eta \, \frac{\nu}{2} \left[1 - \frac{c}{c'} \frac{1 - \nu}{1 - \eta \, \nu} \right], \tag{31}$$

$$\nu_t = \eta \, \frac{\nu}{2} \left[1 + \frac{c}{c'} \frac{1 - \nu}{1 - \eta \, \nu} \right], \tag{32}$$

Hence, the solution immediately after the quench is

$$u(x,t) = \frac{1}{2}\left[1 - \frac{c}{c'}\frac{1-\nu}{1-\eta\,\nu}\right]s\left[x + c'(1-\nu_r)t\right]$$
$$+ \frac{1}{2}\left[1 + \frac{c}{c'}\frac{1-\nu}{1-\eta\,\nu}\right]s\left[x - c'(1-\nu_t)t\right]. \tag{33}$$

The reflection and transmission coefficients are

$$R = \frac{1}{2}\left[1 - \frac{c}{c'}\frac{1-\nu}{1-\eta\,\nu}\right], \qquad T = \frac{1}{2}\left[1 + \frac{c}{c'}\frac{1-\nu}{1-\eta\,\nu}\right], \tag{34}$$

and the height of each chiral profile is

$$U_r = RU, \qquad U_t = TU, \tag{35}$$

where U is the height of the pre-quench soliton.

Since the chiral profiles are not solitons of the post quench dynamics, their shape will change during the evolution, because different parts of each profile will move at different speeds. For short times after the quench, we can take advantage of the fact that each of the reflected and transmitted profiles are similar to the original soliton, just with a reduced height. Thus, we can use (B15) to estimate the velocities of the different parts:

$$V_r = -c' + \frac{\alpha'}{\alpha}c\nu - \left(\zeta' - \frac{\zeta}{R}\frac{\alpha'}{\alpha}\right)u_r(x), \tag{36}$$

$$V_t = c' - \frac{\alpha'}{\alpha}c\nu + \left(\zeta' - \frac{\zeta}{T}\frac{\alpha'}{\alpha}\right)u_t(x), \tag{37}$$

where we used the fact that the width of both profiles is $W = 2\sqrt{\frac{\alpha}{c\nu}}$ and their heights are $U_r = \frac{3}{\zeta}Rc\nu$ and $U_t = \frac{3}{\zeta}Tc\nu$. As a consistency check, we notice that the velocity at the average height of each profile $\left(\langle u_{r,t}\rangle = \frac{1}{3}U_{r,t}\right)$ coincides with (31), (32). The velocities of the profile peaks are

$$V_r^{\text{Peak}} = -c' + 3\frac{\zeta'}{\zeta}Rc\nu - 2\frac{\alpha'}{\alpha}c\nu, \tag{38}$$

$$V_t^{\text{Peak}} = c' - 3\frac{\zeta'}{\zeta}Tc\nu + 2\frac{\alpha'}{\alpha}c\nu, \tag{39}$$

which, in terms of the reduced velocities (30) are

$$\nu_r^{\text{Peak}} = 3\,\nu_r - 2\frac{\eta}{\beta}\,\nu = \left[3 - \frac{2}{\beta_r}\right]\nu_r, \tag{40}$$

$$\nu_t^{\text{Peak}} = 3\,\nu_t - 2\frac{\eta}{\beta}\,\nu = \left[3 - \frac{2}{\beta_t}\right]\nu_t, \tag{41}$$

where

$$\beta \equiv \frac{\Omega_{\zeta'}}{\Omega_{\alpha'}} = \frac{\zeta'}{\alpha'}UW^2 \simeq \frac{\zeta'}{\zeta}\frac{\alpha}{\alpha'}, \tag{42}$$

and

$$\beta_r \equiv R\beta, \qquad \text{and} \qquad \beta_t \equiv T\beta. \tag{43}$$

The parameter $\beta_{r,t}$ characterizes whether the dynamics of the chiral profiles is dominated by the non-linear term of the KdV ($\beta_{r,t} \gg 1$), by the dispersive term ($\beta_{r,t} \ll 1$), or is in the solitonic regime of equilibrium between the two ($\beta_{r,t} \simeq 1$). Equation (42) is obtained considering that before the quench the dimensionless ratio $\frac{\Omega_\zeta}{\Omega_\alpha}$ in (B4) is close to unity, since we prepared the initial state in a solitonic state, and thus the soliton parameter satisfy

$$\frac{\zeta}{\alpha} \simeq \frac{1}{UW^2}. \tag{44}$$

Typically, large quenches $g' \gg g$ gives $\beta \gg 1$ (see, for instance, (52)): we see that the peaks have reduced velocities three times larger than the profile center-of-mass. For smaller quenches, dispersive effects will reduce the peak speeds and we see that for $\beta_{r,t} < 1$, $\nu_{r,t}^{\text{peak}} < \nu_{r,m}$. Moreover, for $\beta_{r,t} < \frac{2}{3}$, the peak starts moving supersonically and thus we expect the profile to become unstable.

Let us now consider the enthalpy $\omega(\rho)$ in (4) to be a simple monomial, that is

$$\omega(\rho) = \phi(g)\rho^{\kappa-1}, \tag{45}$$

then

$$c^2 = (\kappa - 1)\phi(g)\rho_0^{\kappa-1}, \qquad \zeta = \left(\frac{\kappa+1}{2}\right)\frac{c}{\rho_0}, \qquad \text{and} \qquad \eta = 1. \tag{46}$$

Hence

$$\nu_r = \frac{\nu}{2}\left[1 - \frac{c}{c'}\right] = \frac{\nu}{2}\left[1 - \sqrt{\frac{\phi(g)}{\phi(g')}}\right], \qquad R = \frac{1}{2}\left[1 - \frac{c}{c'}\right] = \frac{1}{2}\left[1 - \sqrt{\frac{\phi(g)}{\phi(g')}}\right], \tag{47}$$

$$\nu_t = \frac{\nu}{2}\left[1 + \frac{c}{c'}\right] = \frac{\nu}{2}\left[1 + \sqrt{\frac{\phi(g)}{\phi(g')}}\right], \qquad T = \frac{1}{2}\left[1 + \frac{c}{c'}\right] = \frac{1}{2}\left[1 + \sqrt{\frac{\phi(g)}{\phi(g')}}\right]. \tag{48}$$

Note that the reflection and transmission coefficients are the same of the linear process (15), although the velocities are not.

3.1. Quench protocol for the Gross–Pitaevskii equation

To test the predictions based on the KdV universality, we performed some numerical simulations on physically relevant systems. We consider cold atomic gases with local interaction described by the GP equation

$$i\hbar\,\partial_t\psi = \left\{-\frac{\hbar^2}{2m}\partial_{xx} + f(\rho)\right\}\psi, \tag{49}$$

where $\rho(x, t) = |\psi(x, t)|^2$ and $f(\rho) = g\rho$. To maintain our discussion more general we detail the derivation of the hydrodynamic results for a general $f(\rho)$, but we present numerical results for the GP equation (49) with $f(\rho) = g\rho$. Numerical results for other choices of $f(\rho)$ and in presence of a trapping potential presented in [35] confirm the general validity of the hydrodynamic results for general GP equation with local interactions.

In one dimension, the GP equation reduces to (3), (4) with the ansatz (6). The hydrodynamic functions are

$$\omega(\rho) = \frac{f(\rho)}{m}, \quad \text{and} \quad A = \frac{\hbar^2}{2m^2}. \tag{50}$$

By substituting the hydrodynamic parameters derived in appendices C into 3 for the GP equation we have

$$\frac{c'}{c} = \frac{\zeta'}{\zeta} = \sqrt{\frac{g'}{g}}, \quad \text{and} \quad \eta = 1. \tag{51}$$

Furthermore, remembering the definition (42) of the parameter β we find

$$\beta \propto \left(\frac{c'}{c}\right)^2. \tag{52}$$

Hence, quenching to stronger interactions (higher speed of sound) takes the dynamics to a non-linearity driven regime, as we anticipated.

Using (47), (48) we get

$$\nu_r = R\,\nu, \qquad R = \frac{1}{2}\left[1 - \frac{c}{c'}\right], \tag{53}$$
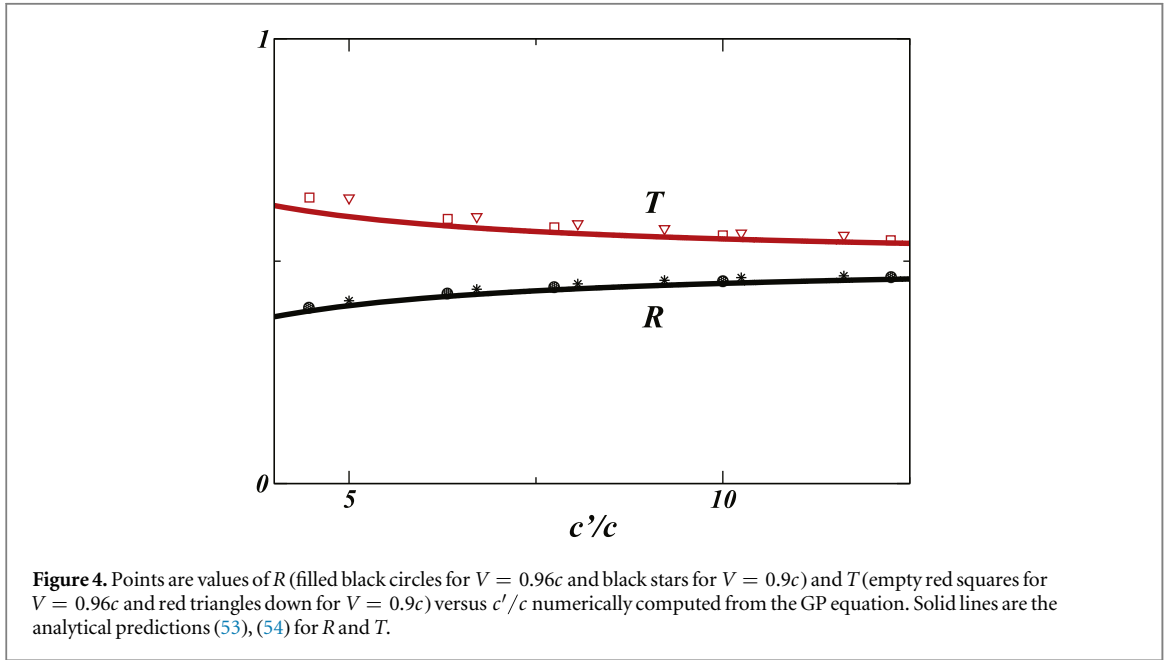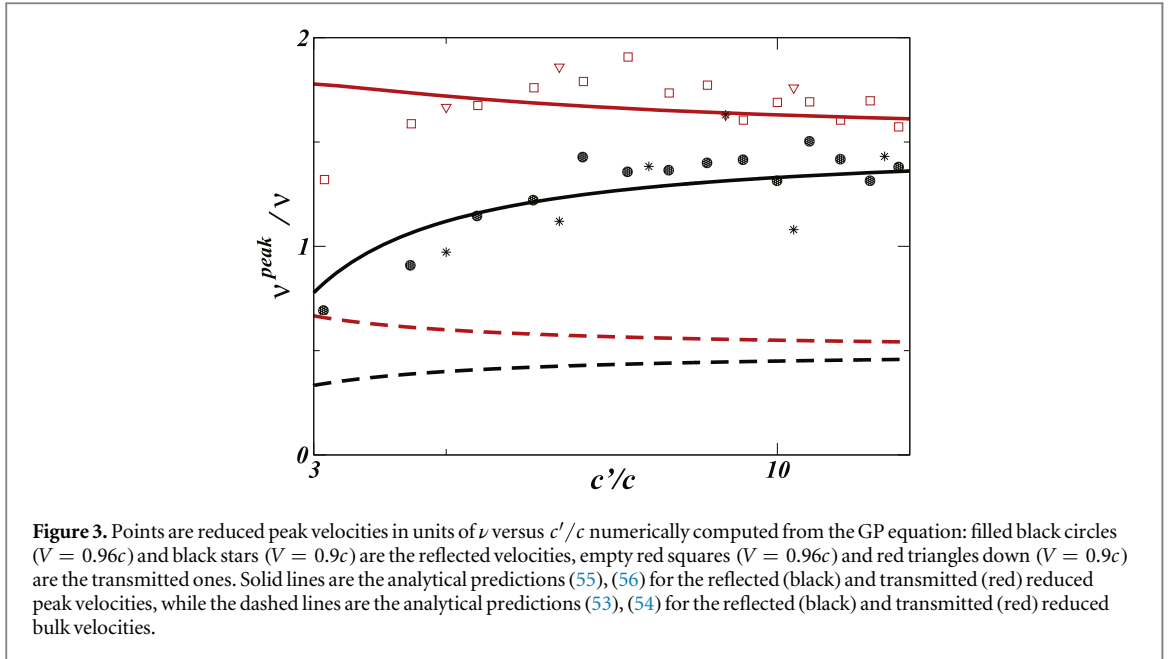
$$\nu_t = T\,\nu, \qquad T = \frac{1}{2}\left[1 + \frac{c}{c'}\right]. \tag{54}$$

For the peak velocities (40, 41) we have

$$\nu_r^{\text{Peak}} = 3\,\nu_r - 2\frac{c^2}{c'^2}\,\nu = \frac{3}{2}\,\nu\left[1 - \frac{c}{c'} - \frac{4}{3}\frac{c^2}{c'^2}\right], \tag{55}$$
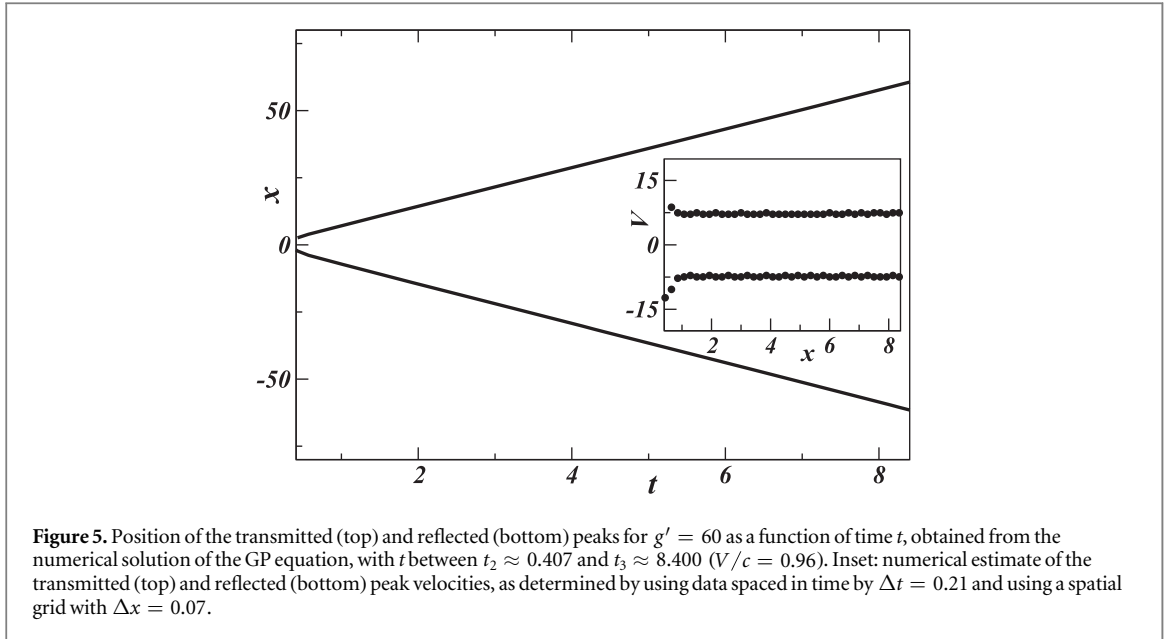
$$\nu_t^{\text{Peak}} = 3\,\nu_t - 2\frac{c^2}{c'^2}\,\nu = \frac{3}{2}\,\nu\left[1 + \frac{c}{c'} - \frac{4}{3}\frac{c^2}{c'^2}\right]. \tag{56}$$

In figure 3 we plot the reduced peak velocities measured during our numerical simulation of the GP equation and compare them to both the prediction for the bulk (53), (54) and peak velocities (55), (56): it is clearly seen that the numerical results discriminate between the two predictions and are rather in agreement with the formulas for the peak velocities. We report in figure 3 numerical data for $V = 0.96c$ and $V = 0.9c$: as expected, numerical data for $V = 0.9c$ are more distant from the analytical predictions, nevertheless the qualitative properties of analytical results (as reduced reflected peak velocities smaller than the transmitted ones and both

Figure 3. Points are reduced peak velocities in units of ν versus c'/c numerically computed from the GP equation: filled black circles ($V = 0.96c$) and black stars ($V = 0.9c$) are the reflected velocities, empty red squares ($V = 0.96c$) and red triangles down ($V = 0.9c$) are the transmitted ones. Solid lines are the analytical predictions (55), (56) for the reflected (black) and transmitted (red) reduced peak velocities, while the dashed lines are the analytical predictions (53), (54) for the reflected (black) and transmitted (red) reduced bulk velocities.

Figure 4. Points are values of R (filled black circles for $V = 0.96c$ and black stars for $V = 0.9c$) and T (empty red squares for $V = 0.96c$ and red triangles down for $V = 0.9c$) versus c'/c numerically computed from the GP equation. Solid lines are the analytical predictions (53), (54) for R and T.

distinct from and larger than bulk velocities) are again visible. While in terms of the reduced velocities the behavior of the peak and the bulk is clearly distinguishable, in natural units the two are dominated by the sound velocity drag. This is the reason for which the data plotted in figure 4 of [35] is well fitted by the bulk prediction as well. In figure 4 we plot, again for $V = 0.96c$ and $V = 0.9c$, the analytical predictions for R and T from (53), (54) and the numerical GP results: the agreement is excellent, even better than for the peak velocities.

The comparison of figures 3 and 4 shows that the hydrodynamic approach gives good results for both bulk and peak velocities, and that the theory can discriminate between them. The data in these figures were taken at time t_{int} defined as halfway between the time t_2 were the two profile become distinguishable after the quench and the time t_3 where the transmitted profile further splits in two. The dynamics around t_3 is clearly beyond our approximation scheme and its treatment requires a different approach, for instance that of [55], which we will not pursue here. Nonetheless, we empirically notice from our numerical experiment that t_3 is more than one order of magnitude greater than t_2. Moreover, as figure 5 shows, the velocities remain approximately constant in this (large) interval of time. The possibility of discriminating peak and bulk velocities is important for experiments, where the bulk velocities could be measured with time-of-flight protocols while peak velocities from *in situ* imaging of the density. Figure 5 guarantees that the results of these measurements is not expected to vary significantly between t_2 and t_3. With typical experimental parameters this means that the experiments

Figure 5. Position of the transmitted (top) and reflected (bottom) peaks for $g' = 60$ as a function of time t, obtained from the numerical solution of the GP equation, with t between $t_2 \approx 0.407$ and $t_3 \approx 8.400$ ($V/c = 0.96$). Inset: numerical estimate of the transmitted (top) and reflected (bottom) peak velocities, as determined by using data spaced in time by $\Delta t = 0.21$ and using a spatial grid with $\Delta x = 0.07$.

should be order of tens/hundreds on *ms*, which is in turn realistic. With the units $\hbar = m = \rho = 1$ for $V/c = 0.96$ we find $t_2 \sim 0.2$–1 and $t_3 \sim 5$–20 for $g' \sim 10$–100. If one considers a confining frequency $\omega_x \sim 2\pi \cdot 10$ Hz, measuring time in units of $1/\omega_x$ one has that $t_3 \sim 1$–10 corresponds indeed to to ~ 10–100 ms. We also observe that a simple estimate of g gives with our units $g \sim 1$ for a transverse frequency of few kHz and a number of particles of order of hundreds (as it is realistic for experiments in which one has many 1*D* tubes).

Using (13), we can estimate the time t_2 at which it is first possible to discern the existence of the two profiles. The comparison with numerical results helps to quantitatively address the validity of the hydrodynamical approach we are following. To do so, we search for the instant at which there is a flex point in (13), that is we look for (x_2, t_2) at which the first and second derivative of (13) vanish:

$$\frac{\mathrm{d}u}{\mathrm{d}x} = \frac{2}{W}[R\tilde{q}(1 - \tilde{q}^2) + T\tilde{p}(1 - \tilde{p}^2)] = 0 , \tag{57}$$

$$\frac{\mathrm{d}^2 u}{\mathrm{d}x^2} = \frac{2}{W}[R(1 - 3\tilde{q}^2)(1 - \tilde{q}^2) + T(1 - 3\tilde{p}^2)(1 - \tilde{p}^2)] = 0 \tag{58}$$

where we introduced

$$q \equiv \tanh[(x - V_r t)/W], \tag{59}$$

$$p \equiv \tanh[(x - V_t t)/W], \tag{60}$$

with $V_{r,t}$ given by (53), (54) and W by (C7).

Once we determine the p and q that solves (57), (58), we have

$$t_2 = \frac{W}{V_t - V_r}(\operatorname{arctanh} q - \operatorname{arctanh} p). \tag{61}$$

Linear combinations of (57), (58) yield the simplified system of equations
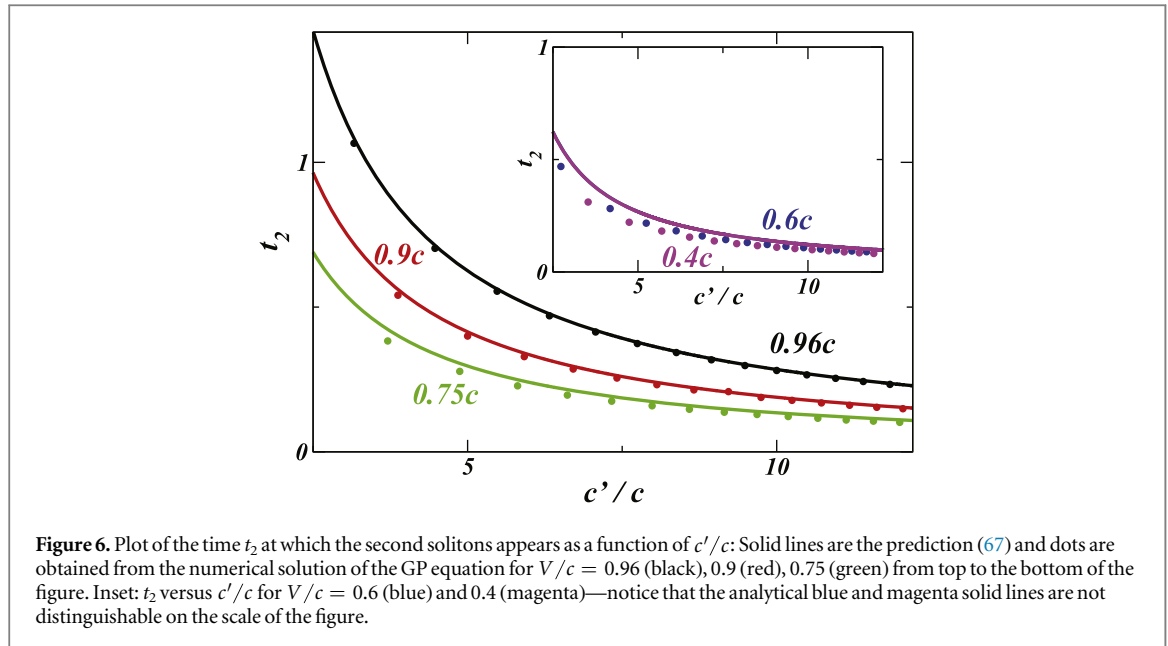
$$Rq(1 - q^2) + Tp(1 - p^2) = 0, \tag{62}$$

$$p(1 - 3q^2) - q(1 - 3p^2) = 0. \tag{63}$$

We can solve (63), for instance, as a quadratic equation in q. One solution is the trivial $q = p$, which corresponds to the equilibrium reached at $x \to \pm\infty$ and is thus not the one we are looking for. The other solution is

$$q = -\frac{1}{3p}. \tag{64}$$

Substituting in (62) we have

$$\frac{1}{27p^3}[R - 9Rp^2 + 27Tp^4 - 27Tp^6] = 0, \tag{65}$$

Figure 6. Plot of the time t_2 at which the second solitons appears as a function of c'/c: Solid lines are the prediction (67) and dots are obtained from the numerical solution of the GP equation for $V/c = 0.96$ (black), 0.9 (red), 0.75 (green) from top to the bottom of the figure. Inset: t_2 versus c'/c for $V/c = 0.6$ (blue) and 0.4 (magenta)—notice that the analytical blue and magenta solid lines are not distinguishable on the scale of the figure.

which can be solved as a cubic equation in p^2. The only real solution is

$$p^2 = \frac{1}{3}\left\{ 1 + 2^{2/3}\left(\frac{c'}{c} + 1\right)^{-1/3}\left[\left(\frac{c'}{c} + 1\right) + \sqrt{\frac{c'^2}{c^2} - 1}\right]^{-1/3} \right.$$
$$\left. + 2^{1/3}\left(\frac{c'}{c} + 1\right)^{-2/3}\left[\left(\frac{c'}{c} + 1\right) + \sqrt{\frac{c'^2}{c^2} - 1}\right]^{1/3} \right\}, \tag{66}$$

where we used the definitions of R, T in (53), (54) in terms of the quench strength $\frac{c'}{c}$.

Substituting this solution into (64) and both of them in (61) and further simplifying the resulting expression we find

$$t_2 = \frac{W}{2(V_t - V_r)} \ln \frac{\sqrt{1 + Q + Q^2} + \frac{\sqrt{3}}{2}(1 + Q)}{\sqrt{1 + Q + Q^2} - \frac{\sqrt{3}}{2}(1 + Q)} \tag{67}$$

where

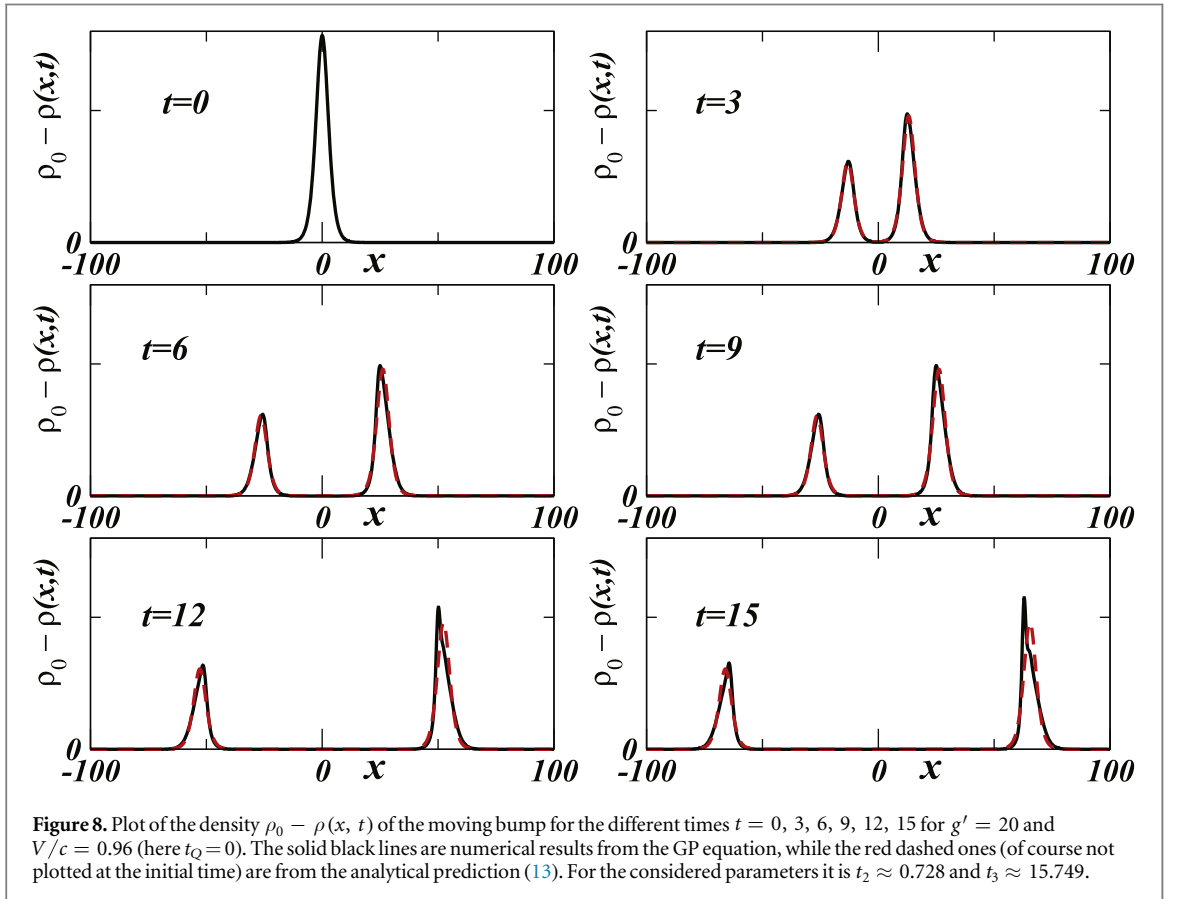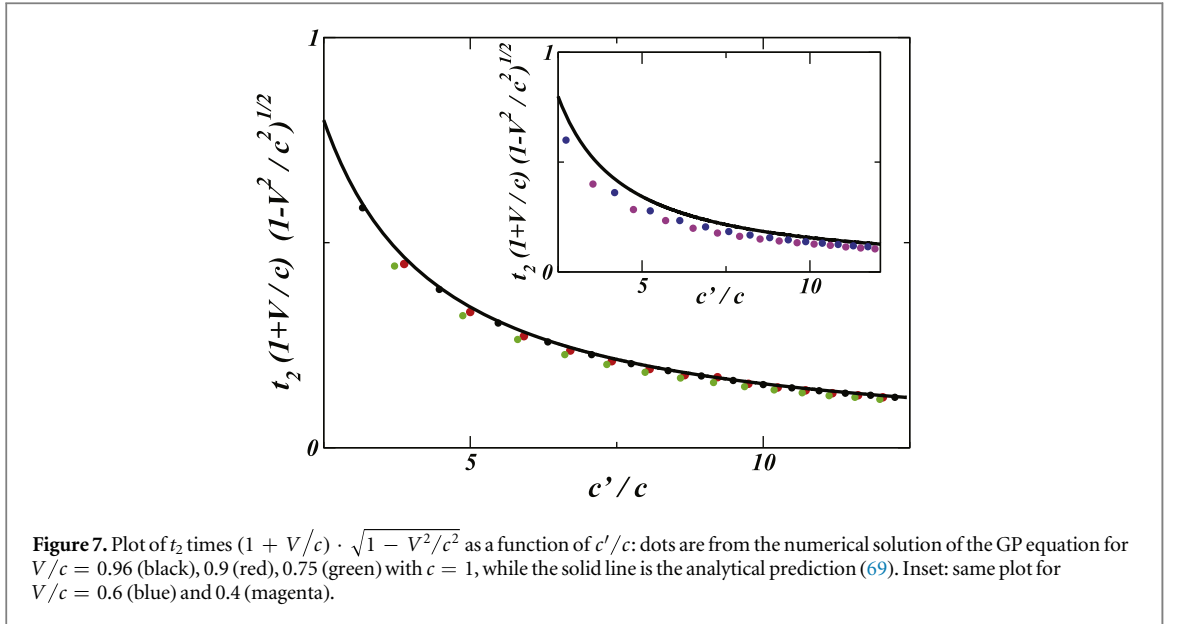$$Q \equiv \left(\frac{c'}{c} + \sqrt{\frac{c'^2}{c^2} - 1}\right)^{2/3}. \tag{68}$$

We tested this prediction against our numerics, finding an excellent agreement and further supporting the validity of our approximation scheme. The comparison is presented in figure 6. As the inset of figure 6 shows, it is seen that the results are rather good also for V/c as low as 0.6 and 0.4, where the KdV approximation for the GPE is not supposed to be reliable.

To quantitatively assess deviations from the prediction (67) we observe that the quantity t_2 times $(1 + V/c) \cdot \sqrt{1 - V^2/c^2}$ according equation (67) itself is independent from the initial velocity:

$$t_2\left(1 + \frac{V}{c}\right)\sqrt{c^2 - V^2} = \frac{1}{2c'} \ln \frac{\sqrt{1 + Q + Q^2} + \frac{\sqrt{3}}{2}(1 + Q)}{\sqrt{1 + Q + Q^2} - \frac{\sqrt{3}}{2}(1 + Q)}. \tag{69}$$

Numerical results for $V/c = 0.96, 0.9, 0.75, 0.6, 0.4$ are reported in figure 7: as expected, one sees that, while for shallow initial solitons the agreement is excellent, by decreasing the initial velocity the agreement becomes less satisfactory, although still acceptable.

To further show how well and for how long the approximations we used remain valid, we plot in figure 8 the density $\rho_0 - \rho(x, t)$ for different times between t_2 and t_3 from the numerical solution of the GP equation and from the KdV hydrodynamic approach. It is seen that the analytical prediction is rather good almost all the way to t_3, even though approaching t_3 it cannot reproduce the deformation needed to expel the third soliton.

Figure 7. Plot of t_2 times $(1 + V/c) \cdot \sqrt{1 - V^2/c^2}$ as a function of c'/c: dots are from the numerical solution of the GP equation for $V/c = 0.96$ (black), 0.9 (red), 0.75 (green) with $c = 1$, while the solid line is the analytical prediction (69). Inset: same plot for $V/c = 0.6$ (blue) and 0.4 (magenta).

Figure 8. Plot of the density $\rho_0 - \rho(x, t)$ of the moving bump for the different times $t = 0, 3, 6, 9, 12, 15$ for $g' = 20$ and $V/c = 0.96$ (here $t_Q = 0$). The solid black lines are numerical results from the GP equation, while the red dashed ones (of course not plotted at the initial time) are from the analytical prediction (13). For the considered parameters it is $t_2 \approx 0.728$ and $t_3 \approx 15.749$.

3.2. Quench protocol for the Calogero model

In the previous section we showed that numerical simulations strongly support our analytical analysis. In this section we perform an additional check, by employing the Calogero model. Details about the Calogero model, its hydrodynamic description and its extension in the presence of an harmonic confinement are in appendices D and E

The study of the interaction quench in the Calogero model allows several different points to be addressed. First, we show that the universality of the quench protocol is robust, in that it applies also to long range interactions such as that of the Calogero model. Additionally, we analyze the effect of an external potential and thus of a non-constant background density. Finally, instead of simulating directly the hydrodynamic of the

model, we perform a (classical) Newtonian evolution for a system composed of a large number of particles and extract the emerging collective behavior. We will see that the initial soliton will split into a reflected and transmitted density profile, showing an emergent wave behavior out of the individual particle dynamics.

The Calogero model in an external harmonic potential is defined by the Hamiltonian [85, 86]

$$H = \frac{1}{2m}\sum_{j=1}^{N}(p_j^2 + \omega^2 x_j^2) + \frac{\hbar^2}{2m}\sum_{j\neq k}\frac{\lambda^2}{(x_j - x_k)^2},\tag{70}$$

with a dimensionless coupling constant λ. We can perform the numerical evolution in the classical limit (in the quantum Calogero models the coupling undergoes the quantum shift $\lambda^2 \to \lambda(\lambda - 1)$), which is integrable even in the presence of an external parabolic potential.

This model has a long-range (power-law) interaction and thus it lies in a different universality class, compared to local models. At the same time, as it was recognized in [53], the potential $1/r^2$ is also relatively short ranged in one dimension (despite being power law). Thus, although such an interaction has not yet been realized in cold atomic gases, this model provides a good platform to study systems beyond contact interaction, with the additional benefit of being exactly solvable, even with an external confinement.

The above model (equation (70)) has been shown to admit soliton solutions in [52]. These are very special set of positions and momenta for each particle that collectively evolve as a robust bump on top of a curved density background (see appendix E).

Due to the power-law interaction, the hydrodynamic description of (70) is not the KdV, but a different integrable equation, in the family of the Benjamin–Ono (BO) equation [87]. It differs from the KdV by its dispersive term and by the fact that its solitons have longer (power-law) tails. Another difference is that this system supports supersonic bright solitons, instead of the subsonic dark ones of local models [52]. We collect in appendices D and E some useful information and new results on the model.

We can calculate the bulk velocities of the reflected and transmitted profiles by operating as before, through the velocity of the center-of-mass of each. Solving the system of equation (22) for this case yields the same results as for the KdV, with $\eta = 1$. To take into account the supersonic nature of the Calogero excitations we define the reduced velocities as

$$V = c(1 + \nu), \qquad V_r = -c'(1 + \nu_r), \qquad V_t = c'(1 + \nu_t),\tag{71}$$

so that ν and $\nu_{r,t}$ are all positive. In terms of these, we have

$$\nu_r = R\nu, \qquad \nu_t = T\nu,\tag{72}$$

and

$$R = \frac{1}{2}\left[1 - \frac{c}{c'}\right], \qquad T = \frac{1}{2}\left[1 + \frac{c}{c'}\right],\tag{73}$$

which coincides with (53), (54).

The solitons in Calogero are Lorentzian (D9) and we notice that their height and width do not depend on the coupling λ. Hence, if β was of the order of unity before the quench, after the quench $\beta_{r,t}$ will be less than unity, proportional to the coefficients R, T, due to the height reduction. Hence, for the Calogero model, after then quench we will be inevitably in the dispersive regime. We can calculate the peak velocities using (D23), with $a_r = R\rho_0\tau, a_t = T\rho_0\tau$:

$$\nu_r^{\text{peak}} = [\zeta'R - 3\pi\alpha'_{\text{BO}}]\frac{\rho_0}{\tau c'} = \left[4 - \frac{3}{R}\right]\nu_r = -\left[1 + 2\frac{c}{c'}\right]\nu,\tag{74}$$

$$\nu_t^{\text{peak}} = [\zeta'T - 3\pi\alpha'_{\text{BO}}]\frac{\rho_0}{\tau c'} = \left[4 - \frac{3}{T}\right]\nu_t = -\left[1 - 2\frac{c}{c'}\right]\nu \ .\tag{75}$$

We see that the reflected peak always move slower than the speed of sound ($\nu_r < 0$ in our notations), while the transmitted one remains supersonic only for $c' < 2c$. This results is seemingly counterintuitive, since the profile densities lie above the background and their bulk velocities are supersonics. While, in a non-linearity dominated regime, the profile peaks would move faster than the bulk, we see that after the quench the Calogero model is in the dispersive regime and thus the peaks move even slower that speed of sound. Thus, while the bulk behavior of the Calogero system after the quench follows the same universality of local models, the peak velocities belong to a different universality.

In our numerical simulation, we used the results of [52], where it was shown that a system on N Calogero particles is dual to a system of M interacting complex parameters, where M counts the number of solitons in the system. Thus, to a system of N particle lying on the real axis and interacting through (70) we add a dual particle $z(t)$ (see appendix E) which draws an ellipse on the complex plane. The interaction of the dual variable with the real particles induces a soliton in the latter and the soliton peak follows the projection of the z particle on the real

axis. As explained in [52], a very useful property of this system is that, given an initial condition for the particle position and momenta, the configuration at any given time *t* can be found exactly by diagonalizing a certain matrix system (by exploiting the Lax pair formulation of the model). In this way, we have been able to set the initial conditions of a soliton, to let it evolve for some time and to follow its evolution after the interaction quench exactly.

In [54] the ground state of the quantum Calogero model in a harmonic potential was studied after a quench and it was observed that the one-particle density starts oscillating and breathing. Such behavior is natural, since after the quench the equilibrium particle distance increases and the trapping cannot compensate for this repulsion. To neutralize this effect, it is thus important to quench at the same time both the interaction and the external potential, so that the background density stays constant. We found that for the model (70) the trapping has to be increased by the same amount of the interaction:

$$\omega' = \frac{\lambda'}{\lambda}\omega. \tag{76}$$

Once we are able to stabilize the background in this way, we perform the quench experiment and measure the characteristics of the reflected and transmitted profiles.

To produce the initial soliton configuration, we specify a given complex number *z* and the initial value problem for the position and momentum of each particle in the system $(x_j(0),\ p_j(0))$ is given by the following equations which can be solved numerically:

$$\omega x_j = \lambda \sum_{k=1(k\neq j)}^{N} \frac{1}{x_j - x_k} - \frac{\lambda}{2}\left(\frac{1}{x_j - z} + \frac{1}{x_j - \bar{z}} \right), \tag{77}$$

$$p_j = i\frac{\lambda}{2}\left(\frac{1}{x_j - z} - \frac{1}{x_j - \bar{z}} \right). \tag{78}$$

Having determined the initial values of $x_j(0)$ and $p_j(0)$, the time dynamics of the system of Calogero particles after the quench can be computed by exploiting the Lax pair formalism, similarly to what was done in [52] to study the dynamics of a harmonic Calogero model soliton. One introduces the following $N \times N$ matrices:

$$X_{ij} = \delta_{ij}x_i, \tag{79}$$

$$L^{\pm} = L \pm i\omega'X, \quad \text{where } L_{ij} = p_i\delta_{ij} + (1 - \delta_{ij})\frac{i\lambda'}{x_i - x_j}, \tag{80}$$

$$M_{ij} = \lambda'\left[\delta_{ij} \sum_{l=1(l\neq i)}^{N} \frac{1}{(x_i - x_l)^2} - (1 - \delta_{ij})\frac{1}{(x_i - x_j)^2} \right], \tag{81}$$

which depend on time through $x_j(t)$ and $p_j(t)$. It is straightforward to show that the equations of motion,

$$\dot{x}_j = p_j, \tag{82}$$

$$\dot{p}_j = -\omega'^2x - \lambda^2\frac{\partial}{\partial x_j}\sum_{k=1\,(k\neq j)}^{N}\frac{1}{(x_j - x_k)^2} \tag{83}$$

are equivalent to the following matrix equations

$$\dot{X} + i[M, X] = L, \tag{84}$$

$$\dot{L} + i[M, L] = -\omega'^2X \tag{85}$$

or equivalently

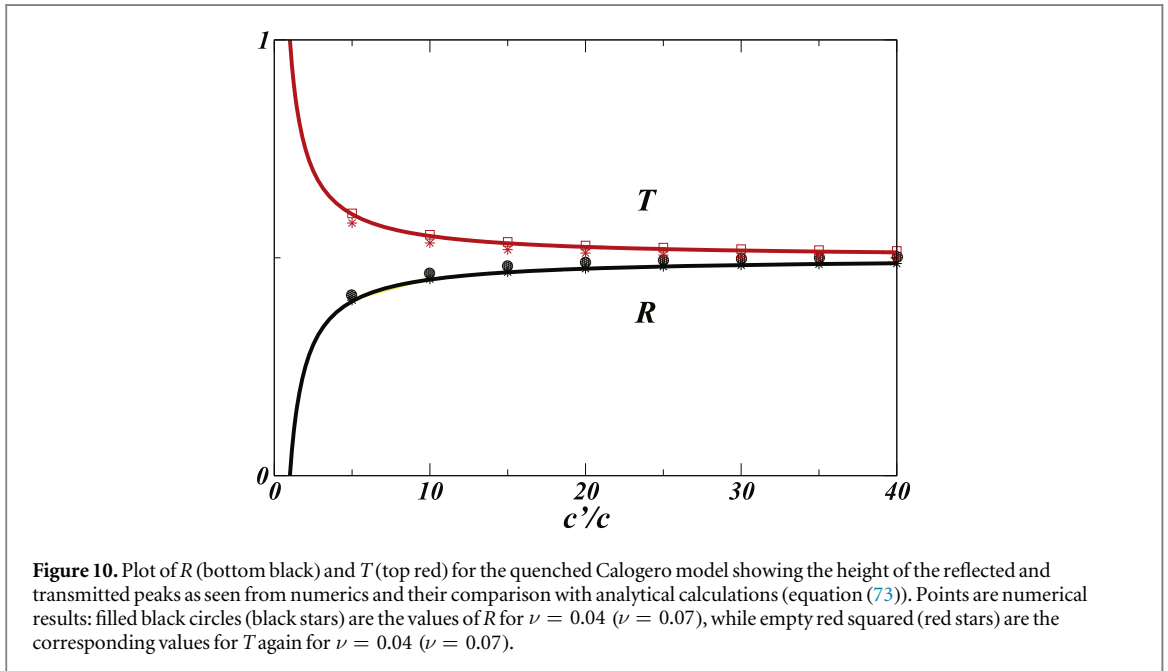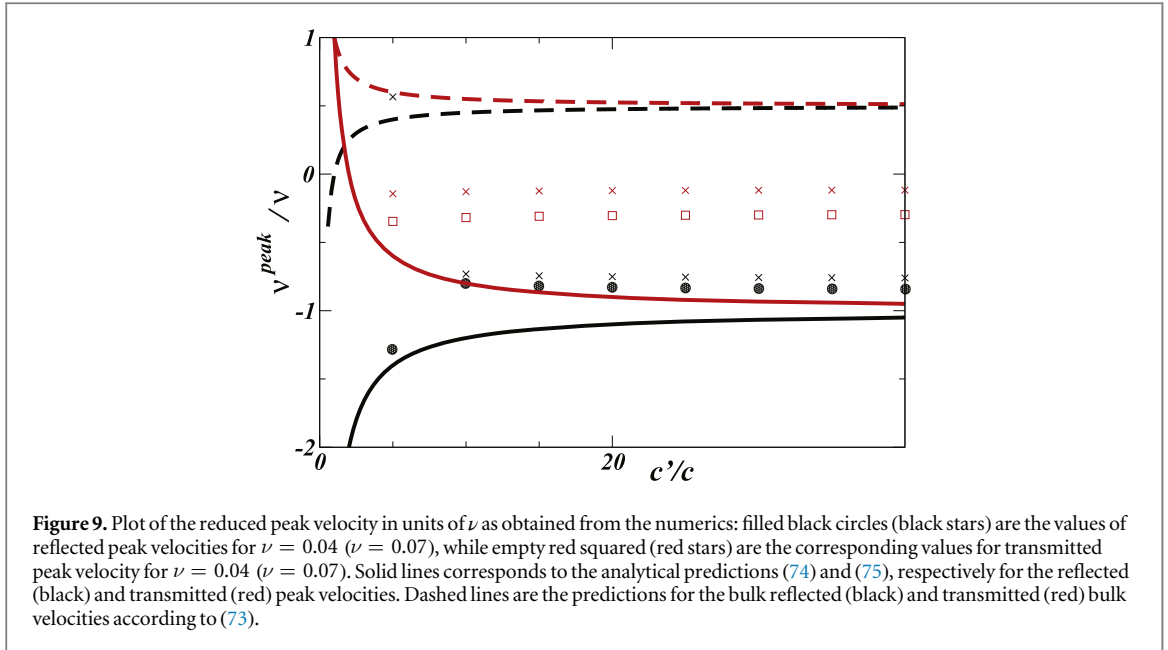$$\dot{L}^{\pm} = -i[M, L^{\pm}] \pm i\omega'L^{\pm} \tag{86}$$

written in terms of *L* and *M* matrices usually referred to as a Lax pair.

One can then write the solution of the harmonic Calogero model as an eigenvalue problem for a matrix which can be explicitly constructed from the initial positions and velocities of the Calogero particles. Namely, the particle trajectories are given by eigenvalues of the following matrix [88]

$$Q(t) = X(0)\cos(\omega't) + \frac{1}{\omega'}L(0)\sin(\omega't), \tag{87}$$

where the matrices $X(0)$ and $L(0)$ are constructed using the initial conditions $x_j(0)$, $p_j(0)$ from (77), (78) inserted in the definitions (79), (80). It is worth pointing out that the above technique is non-iterative in time and hence there is no numerical error accumulation.

In our numerical investigations, we used two different initial soliton velocities: one moving 4% faster than the speed of sound and one 7%. In figure 9 we present results for the reduced (reflected and transmitted) peak

Figure 9. Plot of the reduced peak velocity in units of ν as obtained from the numerics: filled black circles (black stars) are the values of reflected peak velocities for $\nu = 0.04$ ($\nu = 0.07$), while empty red squared (red stars) are the corresponding values for transmitted peak velocity for $\nu = 0.04$ ($\nu = 0.07$). Solid lines corresponds to the analytical predictions (74) and (75), respectively for the reflected (black) and transmitted (red) peak velocities. Dashed lines are the predictions for the bulk reflected (black) and transmitted (red) bulk velocities according to (73).

Figure 10. Plot of R (bottom black) and T (top red) for the quenched Calogero model showing the height of the reflected and transmitted peaks as seen from numerics and their comparison with analytical calculations (equation (73)). Points are numerical results: filled black circles (black stars) are the values of R for $\nu = 0.04$ ($\nu = 0.07$), while empty red squared (red stars) are the corresponding values for T again for $\nu = 0.04$ ($\nu = 0.07$).

velocities for both cases. While the numerical results for the reflected peak velocities are clearly closer to the analytical peak estimates than to the bulk ones, the agreement is less satisfactory for the transmitted peak velocities (the 4% data are closer to the peak velocities, while the 7% data are almost in the middle between the peak and the bulk reduced velocities). Nevertheless, these data are clear evidence of the subsonic dynamics predicted by the analytics above, while evidently the peculiarities of the Calogero model render the quantitative comparison more troublesome. In figure 10, we show the comparison between analytics (equation (73)) and numerics for the reflected and transmitted heights (R, T) for the cases of $\nu = 4\%$ and 7%. A remarkable agreement between these analytical predictions and the numerical calculations performed on the Calogero model is evident.

4. Discussion and conclusions

We have discussed a novel quench protocol, in which a moving, localized excitation reacts to a global interaction quench. We focused on a special class of excitations, namely, soliton solutions, which are stable and experimentally achievable in cold atomic systems as well as in other relevant interacting low-dimensional

systems. We provided a general hydrodynamic framework describing the collective behavior of such systems. Using this hydrodynamic description, we showed that the dynamics immediately after the quench is universal, in that it does not depend on the details of the microscopic interaction, but only on macroscopic quantities, such as the speed of sound before and after the quench.

The quench protocol can be seen as an initial value problem for the non-linear PDE of hydrodynamic type. This has been the approach of [55–57] and is also common in mathematics. It is thus known that a generic initial condition will eventually break into several components, each moving with different velocities (see figure 1). Under certain conditions, some of these components will be stable, while others (most of them) will disperse. In [55] it was noted that, for the integrable non-linear Schrödinger, a quench that brings the new speed of sound to be an integer multiple of the original one will only generate a train of solitons (approximately half of them moving in the same direction as the pre-quench soliton and the other half moving in the opposite direction) and no dispersive sound waves.

In our approach we focused on short times after the quench and, making no assumptions on the integrability of the models, but using the structure of the initial condition provided by the quench protocol, we predict that the initial excitation will immediately break into two counter-propagating packets. While they will eventually break further, for a certain time the two chiral packets will retain the shape of the original excitation, but with amplitudes reduced by a reflection and transmission coefficient. The universal form of these coefficients are given in (28), (29), while the bulk velocities of the two profiles appear in (31), (32). It is also possible to express the latter in dimensionless quantities as in (31), (32). These velocities are measurable in a time of flight experiments, but in our numerical simulation we employ a direct measurement scheme. Thus, it is simpler to measure the velocities of the peak of the profiles, which differ from the bulk (that is, center-of-mass) velocities because of the internal redistribution of energies of the packets. The universal expressions for the peak velocities are given in (40), (41). In figures 3 and 4 we plot the comparison between the analytical expressions and the numerical results obtained through 1D Gross–Pitaevskii equation, which show a good agreement for the R and T coefficients and an acceptable agreement for the peak velocities. As reported in [35], when expressed in natural units, the agreement between the analytical expressions and the numerical data for the velocities is excellent, although it is hard to discriminate between peak and bulk predictions. We also addressed the experimental feasibility of the proposed protocol: in (67) we analytically estimated the time at which the two-profiles dynamics becomes discernible and show in figures 6, 7 its agreement with the numerical data. We also argued that measurements can be performed reliably for around 10–100 ms before intermediate-time effects should be taken into account. Figure 5 shows that in this 'short time' dynamics window the profile velocities stay reasonably constant and figure 8 that the analytical profiles are well fitted by the numerical ones.

We also considered the Calogero model. This model allows us to establish several relevant points. First of all, we see that, despite the non-local nature of this interaction, the short times dynamics remain similar to the local case and we found that the R and T coefficients, as well as the bulk velocities of the chiral profiles, are given by the same universal expression as before. The peak velocities, instead, follow a different universality which is dominated by dispersive effects. While the solitons and the chiral profiles move supersonically in the Calogero case, the peak velocities are predicted to be subsonic. The agreement between the analytical expectations and the numerical simulation are less satisfactory in this case, compared to the local interactions, but still support the qualitative behavior derived analytically and the result for the subsonic peak velocities. In our numerical simulations of the Calogero dynamics we employ a classical, Newtonian evolution of the particles and extracted their collective behavior, whose agreement with the hydrodynamic prediction is a further, somewhat independent, proof of the solidity of our approach.

Finally, the Calogero model remains integrable even in the case of an external harmonic potential. Thus, by including the effect of the trap, we established that by simultaneously quenching the interaction between the particles and the external field, it is possible to keep the background density fixed and isolate the quench dynamics of the soliton. We believe that this observation is applicable to the experimental realization of the protocol and give us insights on how to deal with the external trapping. It would be in our opinion an interesting future work to study the quench dynamics for fermionic systems with long-range couplings or interactions to study the effect of non-trivial Fermi surfaces [89] and the effect of long-rangeness on the formation and propagation of shock-waves [90].

We collected in the appendices some old and new results concerning the dynamics of solitons in non-linear and cold atom systems. There, we explained how the dynamics of shallow profiles can always be captured by the KdV equation and in particular how does this work for the GP equation (and its generalizations). We also considered the solitons for system of Calogero type and discussed their behavior in the presence of an external trap. In this case, the soliton changes its shape during the evolution, because the background density is also changing. We derived the expression for the soliton velocity on such background and showed that it decreases moving toward the edges of the systems as the soliton width is also simultaneously decreasing. Such behavior

contradicts the common wisdom valid in traditional, translational invariant case of constant background (namely, the notion that thinner solitons move faster).

The realizations of low dimensional bosonic gases along with cutting edge technologies available for their manipulation (e.g., the generation of solitons, the induction of interaction quenches, and the observation of the subsequent time dynamics) stimulates the development of theoretical tools to interpret these data. We believe that our work paves the path for new experiments. While we assume a cold atomic gas realization as the natural setting to implement our quench protocol, we should stress that it may be realizable in non-linear optical experiments as well, where the non-linear Schrödinger equation and non-linear PDE are ubiquitous.

Future directions of investigations include studying the consequences of having multiple local excitations (corresponding to multi-soliton profiles) and their subsequent behavior and interactions after the quench. Also systems with multiple species (for e.g, two types of bosons) are realized in low-dimensional cold atomic experiments [91–93] and therefore, investigating the possible mapping to multiple coupled copies of chiral differential equations (for e.g, coupled KdV equations) could be timely and important. Two-component Bose gases may be used for guided matter-wave interferometry [94] and it would be interesting to study applications of the soliton dynamics controlled by interaction quenches to matter-wave interferometry. Understanding the interplay between chiral differential equations could shine light on the complex dynamics of multi-species systems.

Clearly, we think that the comparison of our theoretical results with experimental findings would be very interesting and this will provide input to improve our modeling. A more ambitious future direction would be to study quenches of excited states of quantum systems in regimes where they do not admit a hydrodynamic description and to discuss the behaviour of quantum states that in the hydrodynamical regime behaves like a soliton.

Appendix A. Universality of the KdV equation

The existence of solitons has been foremost an empirical observation [76]. It then took a while to realize that solitons appear as solutions of integrable differential equations. The reason for which solitonic waves can propagate in actual physical systems is that under general assumptions it is possible to isolate an integrable core in the dynamics, while the rest of the terms can often be neglected up to a given time scale. The typical appearance of this 'non-linear universality' is the emergence of the KdV equation as the integrable core of local fluid for shallow waves [76].

In [51] the standard derivation of KdV in classical fluids was reproduced to extend it to the hydrodynamic treatment of cold quantum systems. We review in this appendix their approach, to set the notations that we used in the body of this work.

Our starting point are the continuity and Euler equations (3), which assume no dissipation. The results are not modified qualitatively, as long as dissipative effects enter linearly. We introduce the following notations

$$A_0 = A(\rho_0), \tag{A1}$$

$$\omega_0 = \omega(\rho_0), \tag{A2}$$

$$\xi_\pm = x \pm ct, \tag{A3}$$

with respect to the equilibrium density ρ_0. We want to describe long wave excitations on top of the constant background density ρ_0. Thus we are looking for solutions in the form

$$\rho(x, t) = \rho_0 + \delta\rho_\alpha(\xi_\alpha, t), \tag{A4}$$

$$v(x, t) = \delta v_\alpha(\xi_\alpha, t), \tag{A5}$$

where $\alpha = \pm$ indicates the wave chirality and where we anticipated the fact that small waves will move with velocities close to the sound speed.

The perturbative expansion is based on a counting scheme with formal counting parameter ϵ. We introduce the expansion of velocity and density fields as

$$\delta\rho_\pm(\xi_\pm, t) = \epsilon^2 \rho_\pm^0(\epsilon\xi_\pm, \epsilon^3 t) + \epsilon^4 \rho_\pm^1(\epsilon\xi_\pm, \epsilon^3 t) + \dots \tag{A6}$$

$$\delta v_\pm(\xi_\pm, t) = \epsilon^2 v_\pm^0(\epsilon\xi_\pm, \epsilon^3 t) + \epsilon^4 v_\pm^1(\epsilon\xi_\pm, \epsilon^3 t) + \dots \tag{A7}$$

We substitute this ansatz into (3), (4) and collect terms $\sim\epsilon^3$ and $\sim\epsilon^5$. At cubic order we get

$$v_\pm^0 = \mp\frac{\omega_0'}{c}\rho_\pm^0 \tag{A8}$$

and the consistency

$$c^2 = \rho_0\omega_0'. \tag{A9}$$

At the next order, we can combine the two hydrodynamical equations to get

$$\dot{u}_\pm \mp \zeta u_\pm \partial_x u_\pm \pm \alpha \partial_x^3 u_\pm = 0, \tag{A10}$$

where we introduced

$$\rho_\pm^0 \equiv u_\pm, \tag{A11}$$

$$\zeta \equiv \left(\frac{3\omega_0'}{2c} + \frac{\omega_0''\rho_0}{2c}\right) = \frac{c}{\rho_0} + \frac{\partial c}{\partial\rho_0}, \tag{A12}$$

$$\alpha \equiv \frac{A_0}{4c}. \tag{A13}$$

We also used the identity (A9) so that

$$\frac{\partial c}{\partial\rho_0} = \frac{\omega_0'}{2c} + \frac{\omega_0''\rho_0}{2c} = \frac{c}{2\rho_0} + \frac{\omega_0''\rho_0}{2c}. \tag{A14}$$

Shifting (A10) back from the reference frame moving with the sound velocity to the laboratory frame, we have (9).

In this derivation we considered separately the two chiral sectors. A generic initial condition, however, will consist of both chiralities and, in principle, one should take into account the interaction between them. However, these effects can be neglected since, due to locality, the two sectors interact only when they are overlapping, but this happens for a short time, as they pass through each other with a relative velocity of approximately $2c$.

We have thus shown that the dominant non-linear contributions to the dynamics of shallow, long waves in a generic one-component hydrodynamic system (3) is given by (9), which is known as the integrable KdV equation.

Appendix B. Generalities on KdV

The non-linear term ζ in the KdV (9), pushes the different parts of $u(x, t)$ to move with different velocities, so that small perturbations over the background move close to the speed of sound, while the parts more distant from the asymptotic equilibrium ρ_0 move with higher δV. This term tends to generate a shock-like profile, as the tip of u moves faster than the base. The dispersive, α, term, instead, redistributes the kinetic energy within the u profile and effectively lead to a broadening of the u profile.

We can introduce two time scales capturing the effective strength of these two terms

$$\Omega_\alpha = \alpha W^{-3}, \tag{B1}$$

$$\Omega_\zeta = \zeta U W^{-1}, \tag{B2}$$

where W is the typical width of the disturbance over the background and U is its typical size (note that U has the unit of an inverse length, as it describes the height of a density bump). There are three possible regimes

$$\Omega_\alpha \ll \Omega_\zeta, \qquad \Omega_\alpha \gg \Omega_\zeta \qquad \text{and} \qquad \Omega_\zeta \sim \Omega_\alpha. \tag{B3}$$

Physically, they correspond to a regime of dominant non-linearity (true non-linear KdV dynamics), dominant dispersion with linear evolution (dispersive waves) and solitonic (equilibrium between non-linearity and dispersion). The dimensionless ratio

$$\frac{\Omega_\zeta}{\Omega_\alpha} = \frac{\zeta}{\alpha} U W^2 \tag{B4}$$

distinguish the non-linear $\left(\frac{\Omega_\zeta}{\Omega_\alpha} \gg 1\right)$, the dispersive $\left(\frac{\Omega_\zeta}{\Omega_\alpha} \ll 1\right)$, and the solitonic regimes $\left(\frac{\Omega_\zeta}{\Omega_\alpha} \sim 1\right)$.

The KdV supports true solitons which keep a perfect equilibrium between the non-linear and dispersive effect and thus propagate without changing their shape. The solitons can be both bright (density higher than background) or gray (a depletion in density). In fact, (A10) is invariant under the simultaneous reversal of the sign and chirality of $u_\pm \to -u_\mp$. The single (dark) soliton solutions has the form

$$s(\xi_\pm, t) = -U \cosh^{-2}\left[\frac{\xi_\pm \mp \delta V t}{W}\right],\tag{B5}$$

where $\delta V = c - V$ is the velocity of the soliton (in the sound velocity frame). The height and width of the depletion depend on the soliton velocity as

$$W = 2\sqrt{\frac{\alpha}{\delta V}},\tag{B6}$$

$$U = 3\frac{\delta V}{\zeta}.\tag{B7}$$

The first integrals of motions are

$$I_0 = n = \zeta \int u(\xi, t)\mathrm{d}\xi = -2\zeta U W = -12\sqrt{\alpha \delta V},\tag{B8}$$

$$I_1 = \zeta^2 \int \frac{1}{2}u^2(\xi, t)\mathrm{d}\xi = \frac{2}{3}\zeta^2 U^2 W = -\delta V\; n,\tag{B9}$$

$$I_2 = \zeta^2 \int\left[\alpha u_\xi^2(\xi, t) + \frac{\zeta}{3}u^3(\xi, t)\right]\mathrm{d}\xi = -\frac{4}{15}\zeta^3 U^3 W = \frac{6}{5}\delta V^2\; n,\tag{B10}$$

where we rescaled everything by the right factors of ζ, which sets the scale of the amplitude wave, see (9).

We note that the soliton velocity can be found as the ratio between its momentum I_1 and its 'mass' I_0:

$$\delta V = \zeta\frac{\int \frac{u^2}{2}\mathrm{d}e\xi}{\int u\mathrm{d}\xi},\tag{B11}$$

as can be expected by averaging the nonlinear term in the KdV (A10), see also the comment after (B15).

In section 3 we considered the evolution of an initial condition which is functionally the same as the soliton (B5), but not necessarily with the correct parameters U, W of a soliton. The different parts of the KdV equation give:

$$u_x = \frac{2U}{W}\frac{\sinh[(x - Vt)/W]}{\cosh^3[(x - Vt)/W]},\tag{B12}$$

$$\dot{u} = -Vu_x,\tag{B13}$$

$$u_{xxx} = \frac{4}{W^2}\left(1 + \frac{3u}{U}\right)u_x.\tag{B14}$$

We notice that for an inverse cosh square initial condition every term in the KdV is proportional to its space derivative. Hence, we have

$$cu_x + \zeta uu_x - \alpha u_{xxx} = \left[c - \frac{4\alpha}{W^2} + \left(\zeta - \frac{12\alpha}{UW^2}\right)u(x - Vt)\right]u_x.\tag{B15}$$

For a soliton, $UW^2 = \frac{12\alpha}{\zeta}$ and the terms multiplying u_x become a constant, which equals the soliton velocity. For generic U and W, the terms within parenthesis give the velocity of each part of the profile.

Note that the center-of-mass of a profile of the type (B5), that is the height at which the profile has equal area above and below it, is at a third of its total amplitude. In fact the velocity at $u = U/3$ from (B15) is $c - \frac{\zeta}{3}U = V$, that is, the bulk velocity of the profile.

Appendix C. The non-linear Schrödinger equation and its KdV reduction

The non-linear Schrödinger equation (NLSE) is characterized by the dynamical equation (7). In one dimension, the asymptotic modulus of the field $\lim_{x\to\pm\infty}|\Psi(x, t)|^2 = \rho_0$, which defines the (asymptotic) density of particle, helps in defining the dimensionless parameter

$$\gamma \equiv \frac{m}{\hbar^2}\frac{g}{\rho_0},\tag{C1}$$

which controls the effective strength of the interaction. In the weakly interacting limit $\gamma \ll 1$, the NLSE captures the dynamics of the Lieb–Liniger model, describing an integrable system of one dimensional bosons with contact interaction (see the discussion in section 2).

From (5) we can extract the phenomenological parameters of the KdV as

$$c = \sqrt{\frac{g\rho_0}{m}} = \frac{\hbar}{m}\rho_0\sqrt{\gamma}, \tag{C2}$$

$$\zeta = \frac{3}{2}\sqrt{\frac{g}{m\rho_0}} = \frac{\hbar}{m}\frac{3}{2}\sqrt{\gamma} = \frac{3}{2}\frac{c}{\rho_0}, \tag{C3}$$

$$\alpha = \frac{\hbar^2}{8m^2}\sqrt{\frac{m}{g\rho_0}} = \frac{\hbar}{m}\frac{1}{8\rho_0}\frac{1}{\sqrt{\gamma}}. \tag{C4}$$

The NLSE is also integrable and its single (dark) soliton solutions is [50, 84]

$$\psi(x, t) = \sqrt{\rho_0}\left\{\frac{V}{c} - i\sqrt{1 - \frac{V^2}{c^2}}\tanh\left[(x - Vt)\sqrt{\frac{gm}{\hbar^2}\left(1 - \frac{V^2}{c^2}\right)\rho_0}\right]\right\}. \tag{C5}$$

We have

$$\delta\rho(x, t) = |\psi(x, t)|^2 - \rho_0 = -\left(1 - \frac{V^2}{c^2}\right)\rho_0\cosh^{-2}\left[(x - Vt)\sqrt{\frac{gm}{\hbar^2}\left(1 - \frac{V^2}{c^2}\right)\rho_0}\right]. \tag{C6}$$

We notice that the NLSE soliton has the same functional form as that of the KdV (B5), with width and height given by

$$W = \frac{1}{\sqrt{\frac{gm}{\hbar^2}\left(1 - \frac{V^2}{c^2}\right)\rho_0}} \simeq \frac{1}{\rho_0}\sqrt{\frac{c}{2\gamma\delta V}} + \dots, \tag{C7}$$

$$U = \left(1 - \frac{V^2}{c^2}\right)\rho_0 \simeq 2\frac{\delta V}{c}\rho_0 + \dots, \tag{C8}$$

where we expanded for soliton velocities close to the speed of sound and found consistency with (B6), (B7).

We conclude this section observing that with a power-law non-linearity the NLSE reads

$$i\hbar\,\partial_t\Psi(x, t) = \left\{-\frac{\hbar^2}{2m}\partial_{xx} + g|\psi(x, t)|^{2(\kappa-1)}\right\}\psi(x, t). \tag{C9}$$

If the NLSE is intended to mimic 2-body interactions, this generalization considers κ-body contact interaction, i.e. a term $\frac{g}{2\kappa}|\psi(x, t)|^{2\kappa}$ in the Hamiltonian. The hydrodynamic parameters are in this case

$$\omega(\rho) = \frac{g}{m}\rho^{\kappa-1}, \tag{C10}$$

$$A = \frac{\hbar^2}{2m^2}, \tag{C11}$$

for which we find that the corresponding KdV has

$$c = \sqrt{\frac{(\kappa - 1)g\rho_0^{\kappa-1}}{m}}, \tag{C12}$$

$$\zeta = \frac{\kappa + 1}{2}\sqrt{\frac{(\kappa - 1)g\rho_0^{\kappa-3}}{m}} = \frac{\kappa + 1}{2}\frac{c}{\rho_0}, \tag{C13}$$

$$\alpha = \frac{\hbar^2}{8\,c\,m^2}. \tag{C14}$$

Appendix D. Calogero model

The Calogero model [85, 86] is defined by the Hamiltonian

$$H = \frac{1}{2m}\sum_{j=1}^{N}p_j^2 + \frac{\hbar^2}{2m}\sum_{j\neq k}\frac{\lambda^2}{(x_j - x_k)^2}, \tag{D1}$$

with a dimensionless coupling constant λ. The hydrodynamic description of this model has parameters [51]

$$\omega(\rho) = \frac{\hbar^2 \lambda^2}{m^2} \left[\frac{1}{2}(\pi\rho)^2 + \pi\rho_x^H \right], \qquad (D2)$$

$$A(\rho) = \frac{\hbar^2 \lambda^2}{2m^2}, \qquad (D3)$$

where the superscript H stands for the Hilbert transform:

$$f^H(x) = \frac{1}{\pi} \fint \frac{f(y)}{y - x} \, \mathrm{d}y. \qquad (D4)$$

Due to the long-range nature of the Calogero interaction, its hydrodynamic description does not reduce to a KdV equation, but is given by the so-called *double Benjamin–Ono* [87], which, for small (chiral) profiles reduces to the usual Benjamin–Ono equation

$$u_t \pm [c \, u_x + \zeta u u_x + \alpha_{BO}(u_{xx})^H] = 0, \qquad (D5)$$

with parameters

$$c = \frac{\hbar\pi\lambda}{m} \, \rho_0, \qquad (D6)$$

$$\zeta = 2 \, \frac{\hbar\pi\lambda}{m} = \frac{2c}{\rho_0}, \qquad (D7)$$

$$\alpha_{BO} = \frac{\hbar\lambda}{2m} = \frac{c}{2\pi\rho_0}. \qquad (D8)$$

The one-soliton density profile [95] for the rational Calogero is

$$s_C = \frac{\rho_0 \tau}{[\pi\rho_0(x - Vt)]^2 + \tau^2}, \qquad (D9)$$

where

$$\tau = \frac{c^2}{V^2 - c^2}. \qquad (D10)$$

Note that for this model, the soliton is bright (positive density displacement) and hence its velocity $V > c$ is supersonic. The height and width of (D9) are given by

$$U = \frac{\rho_0}{\tau} = \rho_0 \left(\frac{V^2}{c^2} - 1 \right), \qquad (D11)$$

$$W = \frac{\tau}{\pi\rho_0} = \frac{1}{\pi U}. \qquad (D12)$$

Let us again consider the evolution of an initial profile like (D9), but with generic parameters, such as

$$u = \frac{a}{[\pi\rho_0(x - Vt)]^2 + b^2}. \qquad (D13)$$

We have

$$u_x = -2(\pi\rho_0)^2 \frac{a(x - Vt)}{([\pi\rho_0(x - Vt)]^2 + b^2)^2}, \qquad (D14)$$

$$\dot{u} = -Vu_x, \qquad (D15)$$

$$(u_{xx})^H = \pi\rho_0 \left(\frac{1}{b} - \frac{4b}{a} u \right) u_x. \qquad (D16)$$

Hence, the velocity of each part of the profile can be read from the BO equation as

$$cu_x + \zeta u u_x + \alpha_{BO}(u_{xx})^H = \left[c + \alpha_{BO} \frac{\pi\rho_0}{b} + \left(\zeta - \alpha_{BO} \frac{4\pi\rho_0 b}{a} \right) u \right] u_x. \qquad (D17)$$

We see that for a soliton ($a = \rho_0 b$) the term proportional to u vanishes and the soliton moves with velocity $c\left(1 + \frac{1}{2b}\right)$, or

$$b = \frac{1}{2} \frac{c}{V - c}, \qquad (D18)$$

which reproduces (D10) only to leading order in $\delta V = V - c$. Thus, we notice a mismatch between the parameters of the soliton supported by (D5) and those of the true Calogero soliton (D9), (D10), which is

propagated by the double BO. In the limit of small δV the two approach, in the same way as the KdV is a valid approximation to a local hydrodynamics only for shallow waves.

Similarly to what we did for the KdV, we can find the velocity of the profile (D13) from the conserved quantities, as in (B11). We have

$$\int u \ \mathrm{d}x = \frac{a}{\rho_0 b}, \tag{D19}$$

$$\int \frac{u^2}{2} \ \mathrm{d}x = \frac{a^2}{4\rho_0 b^3}. \tag{D20}$$

Hence, the average height of the profile (D13) is

$$\langle u \rangle = \frac{\int \frac{u^2}{2} \ \mathrm{d}x}{\int u \ \mathrm{d}x} = \frac{a}{4b^2} \tag{D21}$$

and its bulk velocity is

$$V_{\mathrm{av}} = c + \zeta \langle u \rangle = c \left(1 + \frac{a}{2\rho_0 b} \right). \tag{D22}$$

Equation (D13) becomes a soliton of (D5) for $a = \rho_0 b$ and in that case (D22) correctly reproduces (D18). The velocity (D22) coincides with the velocity at the center-of-mass, calculated from (D17) at the height (D21), since at this height the dispersive effects are perfectly balanced and cancel out.

The center-of-mass velocity can be compared with the velocity at the peak by setting $u = a/\tau^2$ in (D17)

$$V^{\mathrm{peak}} = c + \zeta \frac{a}{b^2} - \alpha_{\mathrm{BO}} \frac{3\pi\rho_0}{b} = c \left(1 + \frac{2a}{\rho_0 b^2} - \frac{3}{2b} \right). \tag{D23}$$

Appendix E. Harmonic calogero model

The Calogero interaction remains integrable even when an external harmonic potential is applied, as in (70). Most of what is valid for the rational case considered above remains valid, but the background density is now not constant and follows the famous semicircle law [52]

$$\rho_0(x) = \frac{\omega}{\pi\lambda} \sqrt{R^2 - x^2}, \qquad \text{where} \qquad R \equiv \sqrt{\frac{2\lambda N}{\omega}}. \tag{E1}$$

Thus, the speed of sound is not a constant, since it depends on the local density, and is given by

$$c(x) = \frac{\hbar}{m} \pi\lambda\rho_0(x) = \frac{\hbar}{m} \omega \sqrt{R^2 - x^2}. \tag{E2}$$

We notice that the speed of sound at the center of the trap ($x = 0$) is

$$c = \sqrt{2\lambda\omega N}, \tag{E3}$$

and it decreases as we move from the center.

The soliton solutions of the harmonic model were found recently [52]. They can be thought of as 'Lorentzians'-like (D13) that live on top of the background density (E1):

$$\rho(x, t) = \rho_0(x) + \frac{1}{\pi} \frac{y_1(t)}{[x - x_1(t)]^2 + y_1^2(t)} \tag{E4}$$

$$v(x, t) = -g \frac{y_1(t)}{[x - x_1(t)]^2 + y_1^2(t)}, \tag{E5}$$

where

$$z(t) = x_1(t) + \mathrm{i}y_1(t) \tag{E6}$$

is an external parameter that drives the soliton as it traces an ellipse in the complex plane (see also [52] for further details on the external parameter which we dub as dual variable)

$$z(t) = z(0)\mathrm{e}^{\mathrm{i}\omega t} + \frac{\sin \omega t}{\omega} [P(0) - \mathrm{i}\omega X(0)]. \tag{E7}$$

Here $z(0)$ is the initial position of z_1 in the complex plane and $X = \sum_{j=1}^{N} x_j$, $P = \sum_{j=1}^{N} p_j$ are the center-of-mass and the total momentum of the system at $t = 0$. Without loss of generality, we can take $z(0) = \mathrm{i}b$ with $b > 0$ as initial condition, which also gives $X = 0$. The equation of the ellipse in this case is

$$z(t) = \mathrm{i}b\cos(\omega t) - b\left(1 + \frac{1}{\omega}\sum_j \frac{\lambda}{x_j^2 + b^2}\right)\sin(\omega t), \tag{E8}$$

We see that the initial value b uniquely characterizes the soliton. Combining equations (E4) and (D10), the soliton velocity at the center is given by

$$V = c\sqrt{1 + \frac{1}{\pi b \rho_0(0)}} = c\sqrt{1 + \frac{1}{b}\sqrt{\frac{\lambda}{2\omega N}}}. \tag{E9}$$

The soliton velocity changes as it moves away from the center (i.e, as a function of time). Since the soliton follows the external complex parameter $z(t)$, its velocity matches that of the real part of the dual variable $z(t)$:

$$V(t) = \left[1 + \sum_j \frac{\lambda}{x_j^2 + b^2}\right] b\cos(\omega t). \tag{E10}$$

By inspection of equations (E9) and (E10) we get,

$$V(t) = c\sqrt{1 + \frac{1}{b}\sqrt{\frac{\lambda}{2\omega N}}}\cos(\omega t). \tag{E11}$$

As one can notice from the above equation, the soliton velocity decreases as it moves away from the center. It is also worthwhile noticing that the soliton width, $y_1(t)$, also decreases. Therefore, we have a scenario where a soliton is moving slower, as it becomes thinner. In flat background, thinner solitons move faster and thus we see that the interesting interplay between the non-constant background and the soliton moving on top it contradicts the common wisdom valid in constant background.

References

[1] Bloch I, Dalibard J and Zwerger W 2008 Many-body physics with ultracold gases *Rev. Mod. Phys.* **80** 885

[2] Lamacraft A and Moore J 2012 Potential insights into non-equilibrium behavior from atomic physics *Ultracold Bosonic and Fermionic Gases* (*Contemporary Concepts of Condensed Matter Science*) ed A Fetter *et al* (Oxford: Elsevier) (arXiv:1106.3567)

[3] Greiner M, Mandel O, Haensch T W and Bloch I 2002 Collapse and revival of the matter wave field of a Bose–Einstein condensate *Nature* **419** 51

[4] Kinoshita T, Wenger T and Weiss D S 2006 A quantum Newton's cradle *Nature* **440** 900

[5] Jördens R, Strohmaier N, Günter K, Moritz H and Esslinger T 2008 A Mott insulator of fermionic atoms in an optical lattice *Nature* **455** 204

[6] Chen D, White M, Borries C and DeMarco B 2011 Quantum quench of an atomic mott insulator *Phys. Rev. Lett.* **106** 235304

[7] Trotzky S, Chen Y-A, Flesch A, McCulloch I P, Schollwöck U, Eisert J and Bloch I 2012 Probing the relaxation towards equilibrium in an isolated strongly correlated one-dimensional Bose gas *Nat. Phys.* **8** 325

[8] Gring M, Kuhnert M, Langen T, Kitagawa T, Rauer B, Schreitl M, Mazets I, Smith D A, Demler E and Schmiedmayer J 2012 Relaxation and prethermalization in an isolated quantum system *Science* **337** 1318

[9] Cheneau M, Barmettler P, Poletti D, Endres M, Schauß P, Fukuhara T, Gross C, Bloch I, Kollath C and Kuhr S 2012 Light-cone-like spreading of correlations in a quantum many-body system *Nature* **481** 484

[10] Schneider U *et al* 2012 Fermionic transport and out-of-equilibrium dynamics in a homogeneous Hubbard model with ultracold atoms *Nat. Phys.* **8** 213

[11] Langen T, Geiger R, Kuhnert M, Rauer B and Schmiedmayer J 2013 Local emergence of thermal correlations in an isolated quantum many-body system *Nat. Phys.* **9** 640

[12] Adu Smith D, Gring M, Langen T, Kuhnert M, Rauer B, Geiger R, Kitagawa T, Mazets I, Demler E and Schmiedmayer J 2013 Prethermalization revealed by the relaxation dynamics of full distribution functions *New J. Phys.* **15** 075011

[13] Pagano G *et al* 2014 A one-dimensional liquid of fermions with tunable spin *Nat. Phys.* **10** 198

[14] Braun S, Friesdorf M, Hodgman S S, Schreiber M, Ronzheimer J P, Riera A, del Rey M, Bloch I, Eisert J and Schneider U 2015 Emergence of coherence and the dynamics of quantum phase transitions *Proc. Natl Acad. Sci. USA* **112** 3641

[15] Vidmar L, Ronzheimer J P, Schreiber M, Braun S, Hodgman S S, Langer S, Heidrich-Meisner F, Bloch I and Schneider U 2015 Dynamical quasicondensation of Hard-Core Bosons at finite momenta *Phys. Rev. Lett.* **115** 175301

[16] Preiss P M, Ma R, Tai M E, Lukin A, Rispoli M, Zupancic P, Lahini Y, Islam R and Greiner M 2015 Strongly correlated quantum walks in optical lattices *Science* **347** 1229

[17] Steffens A, Friesdorf M, Langen T, Rauer B, Schweigler T, Hübener R, Schmiedmayer J, Riofrio C A and Eisert J 2015 Towards experimental quantum-field tomography with ultracold atoms *Nat. Comm.* **6** 7663

[18] Langen T, Erne S, Geiger R, Rauer B, Schweigler T, Kuhnert M, Rohringer W, Mazets I E, Gasenzer T and Schmiedmayer J 2015 Experimental observation of a generalized Gibbs ensemble *Science* **348** 207

[19] Jaynes E T 1957 Information theory and statistical mechanics *Phys. Rev.* **106** 620

[20] Deutsch J M 1991 Quantum statistical mechanics in a closed system *Phys. Rev.* A **43** 2046

[21] Srednicki M 1994 Chaos and quantum thermalization *Phys. Rev.* E **50** 888

[22] Calabrese P and Cardy J 2007 Quantum quenches in extended systems *J. Stat. Mech.* **0706** P06008

[23] Rigol M, Dunjko V, Yurovsky V and Olshanii M 2007 Relaxation in a completely integrable many-body quantum System: An Ab initio study of the dynamics of the highly excited states of 1D lattice hard-core bosons *Phys. Rev. Lett.* **98** 050405

[24] Gambassi A and Silva A 2012 Large deviations and universality in quantum quenches *Phys. Rev. Lett.* **109** 250602

[25] Essler F H L, Evangelisti S and Fagotti M 2012 Dynamical correlations after a quantum quench *Phys. Rev. Lett.* **109** 247206

[26] Pozsgay B, Mestyán M, Werner M A, Kormos M, Zarńd G and Takács G 2014 Correlations after quantum quenches in the XXZ spin chain: Failure of the generalized gibbs ensemble *Phys. Rev. Lett.* **113** 117203

[27] Ilievski E, De Nardis J, Wouters B, Caux J- S, Essler F H L and Prosen T 2015 Complete generalized gibbs ensembles in an interacting theory *Phys. Rev. Lett.* **115** 157201

[28] Goldstein G and Andrei N 2015 Equilibration and generalized Gibbs ensemble for hard wall boundary conditions *Phys. Rev. B* **92** 155103

[29] Gogolin C and Eisert J 2016 Equilibration, thermalisation, and the emergence of statistical mechanics in closed quantum systems—a review *Rep. Prog. Phys.* **79** 056001

[30] De Grandi C, Gritsev V and Polkovnikov A 2010 Quench dynamics near a quantum critical point *Phys. Rev. B* **81** 012303

[31] Venuti L C and Zanardi P 2010 Universality in the equilibration of quantum systems after a small quench *Phys. Rev. A* **81** 032113

[32] Iyer D and Andrei N 2012 Quench dynamics of the interacting bose gas in one dimension *Phys. Rev. Lett.* **109** 115304

[33] Karrasch C, Rentrop J, Schuricht D and Meden V 2012 Luttinger-liquid universality in the time evolution after an interaction quench *Phys. Rev. Lett.* **109** 126406

[34] Torre E G D, Demler E and Polkovnikov A 2013 Universal rephasing dynamics after a quantum quench via sudden coupling of two initially independent condensates *Phys. Rev. Lett.* **110** 090404

[35] Franchini F, Gromov A, Kulkarni M and Trombettoni A 2015 Universal dynamics of a soliton after an interaction quench *J. Phys. A: Math. Theor.* **48** 28FT01

[36] Piroli L, Calabrese P and Essler F H L 2016 Multi-particle bound state formation following a quantum quench to the one-dimensional Bose gas with attractive interactions *Phys. Rev. Lett.* **116** 070408

[37] Polkovnikov A, Sengupta K, Silva A and Vengalattore M 2011 Nonequilibrium dynamics of closed interacting quantum systems *Rev. Mod. Phys.* **83** 863

[38] Rigol M, Dunjko V and Olshanii M 2009 Thermalization and its mechanism for generic isolated quantum systems *Nature* **452** 854

[39] Biroli G, Kollath C and Läuchli A M 2010 Effect of rare fluctuations on the thermalization of isolated quantum systems *Phys. Rev. Lett.* **105** 250401

[40] Canovi E, Rossini D, Fazio R, Santoro G and Silva A 2012 Many-body localization and thermalization in the full probability distribution function of observables *New J. Phys.* **14** 095020

[41] Calabrese P, Essler F H L and Fagotti M 2012 Quantum quench in the transverse field ising chain: I. Time evolution of order parameter correlators *J. Stat. Mech.* P07016

[42] Wouters B, Nardis J D, Brockmann M, Fioretto D, Rigol M and Caux J- S 2014 Quenching the anisotropic heisenberg chain: exact solution and generalized gibbs ensemble predictions *Phys. Rev. Lett.* **113** 117202

[43] Bucciantini L, Kormos M and Calabrese P 2014 Quantum quenches from excited states in the Ising chain *J. Phys. A: Math. Theor.* **47** 175002

[44] Silva A 2008 The statistics of the work done on a quantum critical system by quenching a control parameter *Phys. Rev. Lett.* **101** 120603

[45] Diez M, Chancellor N, Haas S, Venuti L C and Zanardi P 2010 Local quenches in frustrated quantum spin chains: global versus subsystem equilibration *Phys. Rev. A* **82** 032113

[46] Stéphan J-M and Dubail J 2011 Local quantum quenches in critical one-dimensional systems: entanglement, the Loschmidt echo, and light-cone effects *J. Stat. Mech.* 08019

[47] Münder W, Weichselbaum A, Goldstein M, Gefen Y and von Delft J 2012 Anderson orthogonality in the dynamics after a local quantum quench *Phys. Rev. B* **85** 235104

[48] Torres-Herrera E J and Santos L F 2014 Local quenches with global effects in interacting quantum systems *Phys. Rev. E* **89** 062110

[49] Forster D 1975 *Hydrodynamic Fluctuations, Broken Symmetry, and Correlation Functions* (Reading, MA: W. A. Benjamin)

[50] Pitaevskii L and Stringari S 2003 *Bose–Einstein Condensation* (Oxford: Oxford University Press)

[51] Kulkarni M and Abanov A G 2012 Hydrodynamics of cold atomic gases in the limit of weak nonlinearity, dispersion and dissipation *Phys. Rev. A* **86** 033614

[52] Abanov A G, Gromov A and Kulkarni M 2011 Soliton solutions of Calogero model in harmonic potential *J. Phys. A: Math. Theor.* **44** 295203

[53] Kulkarni M and Abanov A G 2011 Cold Fermi gas with inverse square interaction in a harmonic trap *Nucl. Phys.* B **846** 122

[54] Rajabpour M A and Sotiriadis S 2014 Quantum Quench of the trap frequency in the harmonic Calogero model *Phys. Rev. A* **89** 033620

[55] Gamayun O, Bezvershenko Y V and Cheianov V 2015 The fate of a gray soliton in a quenched Bose–Einstein condensate *Phys. Rev. A* **91** 031605

[56] Gamayun O and Semenyakin M 2016 Soliton splitting in quenched classical integrable systems *J. Phys. A: Math. Theor.* **49** 335201

[57] Caudrelier V and Doyon B 2015 *The quench map in an integrable Ccassical field theory: nonlinear Schrödinger equation* (arXiv:1512.08767)

[58] Morawetz K 2014 Universal short-time response and formation of correlations after quantum quenches *Phys. Rev. B* **90** 075303

[59] Chiocchetta A, Tavora M, Gambassi A and Mitra A 2015 Short-time universal scaling in an isolated quantum system after a quench *Phys. Rev. B* **91** 220302(R)

[60] Chiocchetta A, Gambassi A, Diehl S and Marino J 2016 Universal short-time dynamics: boundary functional renormalization group for a temperature quench (arXiv:1606.06272)

[61] Landau L D and Lifshitz E M 1975 *Fluid Mechanics* (New York: Pergamon)

[62] Khalatnikov I M 2000 *An Introduction to the Theory of Superfluidity* (New York: Westview)

[63] Castin Y 2004 Simple theoretical tools for low dimension Bose gases *J. Phys. IV France* **116** 89

[64] Pethick C J and Smith H 2008 *Bose–Einstein Condensation in Dilute Gases* 2nd edn (Cambridge: Cambridge University Press) ch 15

[65] Burger S, Bongs K, Dettmer S, Ertmer W, Sengstock K, Sanpera A, Shlyapnikov G V and Lewenstein M 1999 Dark solitons in Bose–Einstein condensates *Phys. Rev. Lett.* **83** 5198

[66] Khaykovich L, Schreck F, Ferrari G, Bourdel T, Cubizolles J, Carr L D, Castin Y and Salomon C 2002 Formation of a matter-wave bright soliton *Science* **296** 1290

[67] Meppelink R, Koller S B, Vogels J M, van der Straten P, van Ooijen E D, Heckenberg N R, Rubinsztein-Dunlop H, Haine S A and Davis M J 2009 Observation of shock waves in a large Bose–Einstein condensates *Phys. Rev. A* **80** 043606

[68] Menotti C and Stringari S 2002 Collective oscillations of a 1D trapped Bose gas *Phys. Rev. A* **66** 043610

[69] Kolomeisky E B, Newman T J, Straley J P and Qi X 2000 Low-dimensional Bose liquids: beyond the Gross-Pitaevskii approximation *Phys. Rev. Lett.* **85** 1146

[70] Salasnich L, Parola A and Reatto L 2002 Effective wave-equations for the dynamics of cigar-shaped and disc-shaped Bose condensates *Phys. Rev. A* **65** 043614

[71] Kim Y E and Zubarev A L 2003 Density-functional theory of bosons in a trap *Phys. Rev. A* **67** 015602

[72] Choi S, Dunjko V, Zhang Z D and Olshanii M 2015 Monopole excitations of a harmonically trapped one-dimensional Bose gas from the ideal gas to the Tonks-Girardeau regime *Phys. Rev. Lett.* **115** 115302

[73] Girardeau M D and Wright E M 2000 Breakdown of time-dependent mean-field theory for a one-dimensional condensate of impenetrable bosons *Phys. Rev. Lett.* **84** 5239

[74] Pustilnik M and Matveev K A 2015 Fate of classical solitons in one-dimensional quantum systems *Phys. Rev.* B **92** 195146

[75] Faddeev L D and Takhtajan L A 1987 *Hamiltonian Methods in the Theory of Solitons* (Berlin: Springer)

[76] Newell A C 1985 *Solitons in Mathematics and Physics* (Philadelphia, PA: SIAM)

[77] Kevrekidis P G, Frantzeskakis D J and Carretero-Gonz/'alez R (ed) 2007 *Emergent Nonlinear Phenomena in Bose–Einstein Condensates* (Berlin: Springer)

[78] Streltsov A I, Alon O E and Cederbaum L S 2011 Death of soliton trains in attractive Bose–Einstein condensates *Phys. Rev. Lett.* **106** 240401

[79] Kaminishi E, Sato J and Deguchi T 2015 Recurrence time in the quantum dynamics of the 1D Bose gas *J. Phys. Soc. Jpn.* **84** 064002

[80] Delande D and Sacha K 2014 Many-body matter-wave dark soliton *Phys. Rev. Lett.* **112** 040402

[81] Sato J, Kanamoto R, Kaminishi E and Deguchi T 2016 Quantum states of dark solitons in the 1D Bose gas *New. J. Phys.* **18** 075008

[82] Lamporesi G, Donadello S, Serafini S, Dalfovo F and Ferrari G 2013 Spontaneous creation of Kibble-Zurek solitons in a Bose–Einstein condensate *Nature Phys.* **9** 656

[83] Yefsah T, Sommer A T, Ku M J H, Cheuk L W, Ji W, Bakr W S and Zwierlein M W 2013 Heavy solitons in a fermionic superfluid *Nature* **499** 426

[84] Novikov S P, Manakov S V, Pitaevskii L P and Zakharov V E 1984 *Theory of Solitons: The Inverse Scattering Methods* (New York: Springer)

[85] Calogero F 1969 Solution of a three-body problem in one dimension *J. Math. Phys.* **10** 2191
Calogero F 1969 Ground state of a one-dimensional N-body system *J. Math. Phys.* **10** 2197
Calogero F 1971 Solution of one-dimensional N-body problems with quadratic and/or inversely quadratic pair potentials *J. Math. Phys.* **12** 419

[86] Sutherland B 1971 Exact results for a quantum many-body problem in one dimension *Phys. Rev.* A **4** 2019
Sutherland B 1972 Exact results for quantum many-body problem in one dimension: II. *Phys. Rev.* A **5** 1372
Sutherland B 1975 Exact ground-state wave function for a one-dimensional plasma *Phys. Rev. Lett.* **34** 1083

[87] Abanov A G, Bettelheim E and Wiegmann P 2009 Integrable hydrodynamics of Calogero-Sutherland model: bidirectional Benjamin-Ono equation *J. Phys.* A **42** 135201

[88] Olshanetsky M A and Perelomov A M 1981 *Classical integrable finite-dimensional systems related to Lie algebras* **71** 313–400 May 1981

[89] Gori G, Paganelli S, Sharma A, Sodano P and Trombettoni A 2015 Explicit Hamiltonians inducing volume law for entanglement entropy in fermionic lattices *Phys. Rev.* B **91** 245138

[90] Bettelheim E, Abanov A G and Wiegmann P 2006 Nonlinear quantum shock waves in fractional quantum Hall edge states *Phys. Rev. Lett.* **97** 246401

[91] Thalhammer G, Barontini G, De Sarlo L, Catani J, Minardi F and Inguscio M 2008 Double species condensate with tunable interspecies interactions *Phys. Rev. Lett.* **100** 210402

[92] Gadway B, Pertot D, Reimann R and Schneble D 2010 Superfluidity of interacting bosonic mixtures in optical lattices *Phys. Rev. Lett.* **105** 045303

[93] Gadway B, Pertot D, Reeves J, Vogt M and Schneble D 2011 Glassy behavior in a binary atomic mixture *Phys. Rev. Lett.* **107** 145306

[94] Stevenson R, Hush M, Bishop T, Lesanovsky I and Fernholz T 2015 Sagnac interferometry with a single atomic clock *Phys. Rev. Lett.* **115** 163001

[95] Polychronakos A P 1995 Waves and solitons in the continuum limit of the calogero-sutherland model *Phys. Rev. Lett.* **74** 5153